Highlights

- The anti-rheumatic drug iguratimod ameliorate osteoporosis of rheumatoid arthritis.
- The impact of iguratimod on osteocytes remained unclear.
- The effects of iguratimod was examined by disuse-induced osteoporosis in mice.
- Iguratimod mitigated hindlimb unloading-induced femur bone mass reduction.
- Iguratimod suppressed early growth response protein 1 expression in osteocytes.
- Inhibiting early growth response protein 1 decreased sclerostin and RANKL expression.
- Iguratimod may offer a novel treatment for disuse-induced osteoporosis.

Original article

Title

Iguratimod suppresses sclerostin and receptor activator of NF-κB ligand production via the extracellular signal–regulated kinase/early growth response protein 1/tumor necrosis factor alpha pathway in osteocytes and ameliorates disuse osteoporosis in mice

Authors

Taihei Miura, MD[a], Yuki Etani, MD, PhD[b], Takaaki Noguchi, MD, PhD[a], Makoto Hirao, MD, PhD[c], Kenji Takami, MD[d], Atsushi Goshima, MD, PhD[e], Takuya Kurihara, MD[a], Yuji Fukuda, MD[a], Nagahiro Ochiai, MD[b], Takashi Kanamoto, MD, PhD[f], Ken Nakata MD, PhD[f], Seiji Okada, MD, PhD[a], and Kosuke Ebina, MD, PhD[a,b,*]

Affiliations

[a]Department of Orthopaedic Surgery, Osaka University Graduate School of Medicine, 2-2 Yamada-oka, Suita, Osaka, 565-0871, Japan

[b]Department of Musculoskeletal Regenerative Medicine, Osaka University Graduate School of Medicine, 2-2 Yamada-oka, Suita, Osaka, 565-0871, Japan

[c]Department of Orthopaedic Surgery, National Hospital Organization Osaka Minami Medical Center, 2-1 Kidohigashi, Kawachinagano, Osaka, 586-8521, Japan

[d]Department of Orthopaedic Surgery, Nippon Life Hospital, 2-1-54 Enokojima, Nishi-ku, Osaka, Osaka, 550-0006, Japan

[e]Department of Orthopaedic Surgery, Osaka Rosai Hospital, 1179-3 Nagasone-cho, Kita-ku, Sakai, Osaka, 591-8025, Japan

[f]Department of Health and Sport Sciences, Osaka University Graduate School of Medicine, 2-2 Yamada-oka, Suita, Osaka, 565-0871, Japan

*Corresponding author:

Phone: +81-6-6879-3552; Fax: +81-6-6879-3559

E-mail: k-ebina@ort.med.osaka-u.ac.jp ORCID: 0000-0002-2426-1024

Funding: None

Abstract

Disuse osteoporosis is a prevalent complication among patients afflicted with rheumatoid arthritis (RA). Although reports have shown that the antirheumatic drug iguratimod (IGU) ameliorates osteoporosis in RA patients, details regarding its effects on osteocytes remain unclear. The current study examined the effects of IGU on osteocytes using a mouse model of disuse-induced osteoporosis, the pathology of which crucially involves osteocytes. A reduction in distal femur bone mass was achieved after 3 weeks of hindlimb unloading in mice, which was subsequently reversed by intraperitoneal IGU treatment (30 mg/kg; five times per week). Histology revealed that hindlimb-unloaded (HLU) mice had significantly increased osteoclast number and sclerostin-positive osteocyte rates, which were suppressed by IGU treatment. Moreover, HLU mice exhibited a significant decrease in osteocalcin-positive cells, which was attenuated by IGU treatment. In vitro, IGU suppressed the gene expression of receptor activator of NF-κB ligand (RANKL) and sclerostin in MLO-Y4 and Saos-2 cells, which inhibited osteoclast differentiation of mouse bone marrow cells in cocultures. Although IGU did not affect the nuclear translocation or transcriptional activity of NF-κB, RNA sequencing revealed that IGU downregulated the expression of early growth response protein 1 (EGR1) in osteocytes. HLU mice showed significantly increased EGR1- and tumor necrosis factor alpha (TNFα)-positive osteocyte rates, which ~~was~~ were decreased by IGU treatment. EGR1

overexpression enhanced the gene expression of TNFα, RANKL, and sclerostin in osteocytes, which was suppressed by IGU. Contrarily, small interfering RNA-mediated suppression of EGR1 downregulated RANKL and sclerostin gene expression. These findings indicate that IGU inhibits the expression of EGR1, which may downregulate TNFα and consequently RANKL and sclerostin in osteocytes. These mechanisms suggest that IGU could potentially be used as a treatment option for disuse osteoporosis by targeting osteocytes.

Keywords

disuse osteoporosis; early growth response protein 1; iguratimod; osteocytes; RANKL; sclerostin

1. Introduction

Osteocytes play a crucial role in regulating the interplay between osteoblast-mediated bone formation and osteoclast-driven bone resorption during bone metabolism driven by mechanical loading [1-3]. Therefore, decreased mechanical loading has been found to promote the development of disuse osteoporosis [3], the risk of which is quite high among individuals with musculoskeletal disorders, such as rheumatoid arthritis (RA) [4-6]. Furthermore, mechanical unloading diminishes the efficacy of existing osteoporosis treatments, such as parathyroid hormone (PTH) analogs and bisphosphonates [7,8]. Hence, therapeutic strategies distinct from conventional osteoporosis treatments are needed for improved prevention of disuse osteoporosis.

Studies have identified various factors associated with disuse osteoporosis. First, sclerostin, a glycoprotein mainly secreted by osteocytes and encoded by the SOST gene, has been found to exert inhibitory effects on bone formation by inhibiting Wnt/β-catenin signaling [9]. Mechanical unloading stimuli ~~has~~ have also been found to increase sclerostin expression,

thereby inhibiting bone formation [1,10]. Second, evidence has shown that the receptor activator of NF-κB ligand (RANKL), a type II membrane protein primarily expressed in osteoblasts and osteocytes, induces osteoclastic differentiation and is upregulated by several mechanical unloading–related factors, including sclerostin and tumor necrosis factor (TNF)-α [11,12]. Moreover, one study found that osteoprotegerin (OPG), a decoy receptor for RANKL that inhibits bone resorption, was one of the target genes involved in Wnt/β-catenin signaling [13]. Taken together, accumulated evidence suggests that mechanical unloading may promote sclerostin and RANKL expression and decrease OPG expression, thereby suppressing bone formation and increasing bone resorption. The third cause involves the NF-κB pathway. Reports have shown that mechanical unloading upregulates the NF-κB pathway, which consequently increases the expression of TNFα, RANKL, and SOST in osteocytes [14,15].

A recent meta-analysis reveals that Janus kinase inhibitors (JAKi) and biological disease-modifying antirheumatic drugs (bDMARDs) showed some positive effects on bone metabolism, although had no significant impact on BMD and fracture prevention~~A recent meta-analysis revealed that Janus Kinase inhibitors and biological disease-modifying antirheumatic drugs had no significant impact on bone mineral density and fracture prevention~~ [16,17,18]. However, other studies have shown that iguratimod (IGU), a synthetic small molecule disease-modifying antirheumatic drug, prevented bone loss and improved bone metabolisms in patients with RA [19~~18~~] while inhibiting RANKL-induced osteoclast differentiation [20~~19~~]. Moreover, we previously reported that IGU promoted bone morphogenetic protein-2 (BMP2)-induced bone formation [21~~20~~] and reduced glucocorticoid-induced disorder of bone metabolism in vitro [22~~21~~]. However, considering the lack of relevant studies, the effects of IGU on osteocytes have remained unclear. Therefore, the current study aimed to investigate the effects of IGU specifically on osteocytes utilizing a mouse model of disuse osteoporosis.

2. Materials and methods

2.1 Experimental design and animal model

Eight-week-old male C57BL/6J mice were purchased from Charles River Laboratories (Osaka, Japan). All mice were kept in a temperature- and humidity-controlled facility with a 12-h light/dark cycle and free access to food and water. After a week of acclimatization, the mice were randomly assigned into three groups (Fig. 1A): (1) normal saline (NS) mice (rest + NS injections; n = 8); (2) hindlimb-unloaded (HLU) + NS mice (HLU + NS injections; n = 8); and (3) HLU + IGU mice (HLU + IGU injections; n = 8). NS and IGU (30 mg/kg per day) were injected intraperitoneally five times a week. The mice in the HLU + NS and HLU + IGU groups were suspended by their tails for 21 days using tail suspension clips (Yamashita Giken, Tokushima, Japan) to prevent their hindlimbs from weight-bearing loads (Supplementary Fig. 1A). The tail suspension maintained a head-down tilt of 30°, ensuring that their hindlimbs did not touch the cage floor, as previously described [2322]. The forelimbs remained in contact with the cage bottom, enabling the mice to move freely within a 360° range of motion. To assess the effects of tail suspension on their general body condition, the body weight of the mice was measured daily after initiating tail suspension (Fig. 1B).

For euthanasia and bone sample collection, the mice were anesthetized with an intraperitoneal injection of medetomidine (0.3 mg/kg), midazolam (4.0 mg/kg), and butorphanol (5.0 mg/kg), as previously described [2423]. The left femurs were harvested and used for microcomputed tomography (μCT) and histological analyses.

2.2 Microcomputed tomography

The distal femurs of the mice were scanned using a high-resolution μCT scanner (SkyScan 1272; Bruker, Kontich, Belgium) with a voxel size of 8 μm. The region of interest for analysis was defined as a region ranging from 500 to 1,500 μm proximal to the growth plate,

in which both condyles were no longer visible, and was imaged using 125 slices. Raw images were reconstructed into three-dimensional cross-sectional datasets using a cone beam algorithm with the SkyScan reconstruction software (NRecon, Bruker). Structural indices were then calculated on the reconstructed images using the Skyscan CT Analyzer (CTAn) software (Bruker). A custom processing algorithm was utilized with the CTAn to separate trabecular and cortical bone based on the different thicknesses of the structures. Trabecular parameters included the bone volume fraction (bone volume [BV]/total volume [TV]) and trabecular number (Tb.N), thickness (Tb.Th), and separation (Tb.Sp), whereas cortical parameters included cortical thickness (Ct.Th).

2.3 Histological analysis

After μCT, the femurs were fixed in formalin and decalcified for embedding. Tartrate-resistant acid phosphatase (TRAP) staining was performed according to the manufacturer's protocol (Cosmo Bio, Tokyo, Japan). The number of TRAP-positive cells per trabecular surface was then counted as previously described [24~~23~~].

2.4 Immunohistochemical analysis

Samples were incubated with the following primary antibodies: antiosteocalcin (Takara Bio, Shiga, Japan), antisclerostin (R&D Systems, Minneapolis, MN, United States), antiearly growth response protein 1 (EGR1) (Proteintech, Chicago, IL, United States), anti-Heme Oxygenase 1 (HO-1) (Abcam, Cambridge, MA, United States) and anti-TNFα antibody (LifeSpan BioSciences, Seattle, WA, United States). The sections were then incubated with a secondary antibody (Histofine Simple Stain Mouse MAX PO; Nichirei Bioscience Inc., Tokyo, Japan) and stained with 3,3′-Diaminobenzidine tetrahydrochloride (Dako, Tokyo, Japan). As with μCT, the region of interest for analysis was defined as a region ranging from 500 to 1,500

μm proximal to the growth plate [2423]. Within the region of interest, the number of osteocalcin-positive cells was measured on five randomly selected trabecular bone surfaces, while the percentage of sclerostin-positive osteocytes, EGR1-positive osteocytes, and TNFα-positive osteocytes were evaluated for all osteocytes in the cortical bone. The number of HO-1 positive cells within the trabecular bone region of interest was measured using the Image J software.

2.5 Histomorphometrical analysis

To label active bone formation, all mice were subcutaneously injected with tetracycline (20 mg/kg) and calcein (10 mg/kg) 5 and 2 days before being sacrificed, respectively, as previously described [2524]. The left femurs were extracted, fixed in 70% ethanol, treated with Villanueva bone stain, and embedded in methacrylate (Wako Pure Chemical Industries, Osaka, Japan). Thereafter, the following histomorphometric parameters were quantified: bone formation rate per total volume (BFR/TV) and eroded surface per bone surface (ES/BS)

2.6 Reagents and cell culture

IGU was provided by Toyama Chemical Co. Ltd (Tokyo, Japan) and dissolved in dimethyl sulfoxide (DMSO; Wako Pure Chemical Industries). Approximately, the serum concentration of IGU was reported to reach 3 μg/mL in clinical dose for humans [2221]. We used osteocyte-like cell line MLO-Y4, human osteosarcoma cell line Saos-2 cells, and osteoblastic cell line MC3T3-E1 cells. MLO-Y4 cells were purchased from Kerafast (Boston, MA, United States), whereas Saos-2 and MC3T3-E1 cells were acquired from Riken Cell Bank (Tsukuba, Japan).

MLO-Y4 cells were cultured on type I collagen-coated dishes (Corning, Corning, New

York, United States) in α-minimum essential medium (α-MEM; Nacalai Tesque, Kyoto, Japan) supplemented with 5% heat-inactivated fetal bovine serum (FBS; Hyclone, Logan, UT, United States), 5% calf serum (Hyclone), and 1% antibiotic/antimycotic solution (A/A; Sigma-Aldrich, St. Louis, MO, United States), as previously described [22~~21~~]. Adherent cells were seeded into 24-well plates at 1×10^5 cells/well. After 24 h, the cells were treated with/without 10 ng/mL of TNFα (R&D Systems) and different concentrations of IGU for 5 days.

Saos-2 cells were cultured with Dulbecco's Modified Eagle Medium (Nacalai Tesque, Kyoto, Japan) containing 10% FBS and 1% A/A in 24-well plates at 1×10^5 cells/well. After 24 h, the cells were treated with/without 100 ng/mL of BMP2 (Osteofarmer, Osaka, Japan) and different concentrations of IGU in media containing 5 mM of β-glycerophosphate (Calbiochem, San Diego, CA, United States), and 50 μg/mL of ascorbic acid (Sigma-Aldrich) for 6 days, as previously described [26~~25~~].

MC3T3-E1 cells were cultured with α-MEM containing 10% FBS and 1% A/A in 24-well plates at 1×10^5 cells/well. After 24 h, the cells were treated with/without 10 ng/mL BMP6 (R&D Systems), 100 ng/mL of recombinant mouse sclerostin protein (R&D Systems), and 3 μg/mL of IGU in media containing 10 mM β-glycerophosphate and 50 μg/mL ascorbic acid to induce osteoblast differentiation for 3 days, as previously described [27~~26~~].

2.7 Coculture of MLO-Y4 cells and murine primary osteoclasts

MLO-Y4 cells were seeded at 1,000 cells/cm^2 in a type I collagen-coated 96-well plate. After a 24-h incubation period, the cells were treated with TNFα (10 ng/mL) and various concentrations of IGU. Murine primary osteoclasts were obtained from bone marrow cells flushed from the femurs and tibiae of 8-week-old male C57BL/6J mice. These cells were then cultured overnight in α-MEM supplemented with 10% FBS, 1% A/A, and 10 ng/mL of macrophage colony-stimulating factor (M-CSF; R&D Systems) at 37 °C in a humidified

atmosphere of 5% carbon dioxide, as previously described [2221]. Adherent cells were added at 2,500 cells/cm^2 to the same 96-well plates seeded with MLO-Y4 cells and then cocultured in α-MEM medium supplemented with 10% FBS and 1% A/A. The medium was replaced every 2 days. On day 7, the cells were fixed and stained for TRAP.

2.8 RNA extraction, first‐strand complementary DNA synthesis, and reverse transcription quantitative polymerase chain reaction (RT-qPCR)

Total RNA was extracted from cells treated in a 24-well plate using the RNeasy Mini kit (Qiagen, Düsseldorf, Germany). First-strand complementary DNA was synthesized from 1 μg of total RNA using the ReverTra Ace qPCR RT kit (Toyobo Co., Ltd., Osaka, Japan) following the manufacturer's protocol. RT-qPCR was performed using Fast SYBR Green Master Mix (Life Technologies, Carlsbad, CA, United States) and a Step One Plus Real-Time PCR System (Life Technologies). Gene expression levels were normalized to glyceraldehyde-3-phosphate dehydrogenase, whereas fold changes were calculated relative to the control group using the $2^{-\Delta\Delta Ct}$ method. The PCR primer sequences are described in the Supplementary Table.

2.9 Alkaline phosphatase (ALP) activity assay

ALP activity was assessed by measuring the release of p-nitrophenol from p-nitrophenylphosphate at pH 9.8 using the ALP assay kit (FUJIFILM Wako Pure Chemical Co., Osaka, Japan) in accordance with the manufacturer's protocol. The optical density at 405 nm was monitored to quantify the amount of p-nitrophenol released. The activity was normalized to the protein content assessed using the Pierce™ Bicinchoninic acid（BCA） Protein Assay Kit (Thermo Fisher, Waltham, MA, United States).

2.10 Western blotting

Western blotting was conducted as previously described [2221]. Cytoplasmic and nuclear extracts were prepared using the NE-PER nuclear and cytoplasmic extraction kit (Pierce, Rockford, IL, United States) according to the manufacturer's protocol.

The primary antibodies were as follows: phosphate anti-p38 antibody (Thr180/Tyr182) (1:1,000), anti-p38 antibody (1:1,000), phosphate antistress-activated protein kinase (SAPK)/Jun amino-terminal kinase (JNK) antibody (Thr183/Tyr185) (1:1,000), anti-SAPK/JNK antibody (1:1,000), phosphate anti-NF-κB p65 (1:1,000), anti-NF-κB p65 (1:1,000), phosphate antiextracellular signal–regulated kinase 1/2 (ERK1/2; Thr202/Tyr204) (1:2000), anti-ERK1/2 (p44/42) (1:1,000), β-actin (1:2000), and Lamin-B1 (1:1,000) antibody purchased from Cell Signaling Technology (CST, Danvers, MA, United States). Antisclerostin antibody (1:1,000) was acquired from R&D Systems.

2.11 Luciferase assay

For transient transfection, 1×10^6 Saos-2 cells were suspended in 100 μL of Opti-MEM medium (Thermo Fisher) and electroporated using NEPA21 Super Electroporator (Nepa Gene, Chiba, Japan) at 175 V and a poring pulse length of 5 ms. The cells were then transfected with κB-Luc2P (pGL4.15; Promega, Madison, WI, United States). After electroporation, 3×10^4 cells were seeded into 96-well plates. Following a 24-h incubation period, the cells were treated with or without TNFα, BMP2, IGU, and dexamethasone (Dex; Sigma-Aldrich). Luciferase activity was measured 8 h after treatment using a Centro XS3 LB 960 Microplate Luminometer (Berthold Technologies, Bad Wildbad, Germany) equipped with the Steady-Glo® luciferase assay system (Promega) following the manufacturer's protocol. Luciferase activity was normalized to the protein content measured by the PierceTM BCA Protein Assay Kit (Thermo Fisher).

2.12 Immunofluorescence staining

Saos-2 cells were cultured in a 96-well plate at 5.0×10^3 cells/well. After 24 h of incubation, the cells were treated with/without BMP2 and IGU. After 24 h of treatment, the cells were fixed with paraformaldehyde for 30 min and blocked with 5% rabbit serum for 1 h. Subsequently, the cells were incubated overnight at 4 °C with an anti-p65 antibody (CST, 1:1,000), incubated with antirabbit Alexa Flour 594 (CST, 1:1,000) at room temperature for 1 h in the dark, and counterstained with antifade mounting medium with Hoechst 33258 (Dojindo, Kumamoto, Japan). Cell images were acquired using an IN Cell Analyzer 6000 (GE Healthcare, Chicago, IL, United States), capturing 16 view fields per well. The Nuc/Cyto ratio of the NF-κB signal was calculated using the mean signal intensity of nuclear areas and cytoplasmic areas in cells of each field per well.

2.13 RNA sequencing

Cells underwent total RNA extraction using the RNeasy Mini kit (Qiagen) following the manufacturer's protocol. RNA-Seq libraries were then generated using the TruSeq stranded mRNA sample prep kit (Illumina, San Diego, CA, United States) according to the manufacturer's instructions. Sequencing was performed on an Illumina NovaSeq 6000 platform in the 100-bp single-end mode. The obtained reads were aligned to the human reference genome sequences (hg19) using TopHat version 2.0.13 in combination with Bowtie2 version 2.2.3 and SAMtools version 0.1.19. The number of fragments per kilobase of exon per million mapped fragments was calculated using Cufflinks version 2.2.1. Differential gene expression analysis between groups was conducted using iDEP with a false discovery rate threshold of <0.1 and a fold-change of >1.5. Volcano plot representation and Gene Ontology enrichment analysis were performed using BioJupies, with adjusted p values of <0.05 and absolute log2 fold-change of >1.

2.14 Transient transfection

Saos-2 cells were transfected with small interfering RNA (siRNA) targeting Egr1 (Thermo Fisher), siRNA control (Thermo Fisher), and the EGR1 overexpression vector, pCMV6-EGR1 (pEGR1; OriGen, Rockville, MD, United States). Thereafter, the cells underwent electroporation for transfection and were then seeded into 24-well plates. Following a 24-h incubation period, RT-qPCR analyses were performed to ascertain the correct clone targeting.

2.15 Statistical analysis

All numerical data were reported as mean ± standard deviation and analyzed using Prism software (GraphPad Prism for Windows, version 9.0, San Diego, CA, United States). An unpaired Student's t-test was used for comparisons between two groups, whereas one-way analysis of variance followed by Tukey's post-hoc test was used for comparisons between more than three groups. A p value of <0.05 indicated statistical significance.

2.16 Study approval

All experimental protocols comply with the ARRIVE guidelines and were approved by the Ethics Review Committee for Animal Experimentation of Osaka University Graduate School of Medicine (permission number 02-057-007).

3. Results

3.1 Effects of IGU on disuse osteoporosis in HLU mice

The mice were randomly assigned into three groups: NS, HLU + NS, and HLU + IGU mice (Fig. 1A). All mice subjected to hindlimb unloading successfully completed the 21-day

unloading period. During this unloading period, the body weight of HLU + NS and HLU + IGU mice remained consistently lower than that in the NS group. However, no significant differences were observed among the three groups on day 21 (Fig. 1B).

μCT was utilized to analyze the trabecular and cortical bone of the distal femurs. Representative images of the trabecular bone of mice in each group are presented in Fig. 1C. Analysis of the trabecular bone characteristics showed that the BV/TV, Tb.N, and Tb.Th were significantly lower in HLU + NS mice than NS mice. In contrast, Tb.Sp was significantly higher in HLU + NS mice than in NS mice. IGU treatment in HLU mice prevented BV/TV loss and Tb.N reduction (Fig. 1D). Representative images of the cortical bone of mice in each group are shown in Supplementary Fig. 1B. Analysis of the cortical bone characteristics in the diaphyseal region showed that Ct.Th was also significantly lower in HLU + NS mice than in NS mice. Although IGU treatment appeared to impede this cortical bone loss in HLU mice, it did not promote a significant difference (Supplementary Fig. 1C).

TRAP staining of osteoclasts in the trabecular and cortical bone of the distal femur (Fig. 2A) revealed significantly more TRAP-positive multinuclear cells in HLU + NS mice than in NS mice, with IGU administration attenuating this increase. Subsequently, the effects of HLU and IGU on osteoblastic differentiation ~~was~~ were evaluated. Immunostaining of osteocalcin showed significantly fewer osteocalcin-positive cells in HLU + NS mice than in NS mice (Fig. 2B), with IGU treatment attenuating this reduction. Additionally, sclerostin immunostaining was performed on osteocytes to investigate the effects of HLU and IGU on osteocytes. The ~~percentate~~ percentage of sclerostin-positive osteocytes was significantly higher in HLU + NS mice than in NS mice (Fig. 2C). IGU administration in HLU mice attenuated the increase in the percentage of sclerostin-positive osteocytes.

Figs. 2D, E, and G presents the histomorphometry of the distal femur. Compared to NS mice, HLU + NS mice demonstrated short, thin trabeculae with scattered, small trabecula,

which were recovered by IGU administration (Figs. 2D, E).

In terms of bone formation, BFR/TV tended to be lower in HLU + NS mice than in NS mice (Fig. 2F). IGU treatment in HLU mice tended to attenuate this reduction but not significantly. Regarding bone resorption, HLU + NS mice exhibited significantly higher ES/BS values than did NS mice. Conversely, HLU + IGU mice showed significantly lower ES/BS values than did HLU+NS mice (Figs. 2G, H).

3.2 Effects of IGU on osteocytes and osteoclastogenesis/osteoblastogenesis through osteocytes in vitro

Previous studies have demonstrated that mechanical unloading promotes TNFα, BMP2, RANKL, and sclerostin expression from bone tissues [1,10,28~~27~~,29~~28~~]. RT-qPCR results exhibited that TNFα-treated osteocyte cell line MLO-Y4 showed markedly increased RANKL expression and decreased OPG expression, which significantly increased the RANKL/OPG ratio. IGU treatment significantly inhibited this upregulation of RANKL expression, which significantly decreased the RANKL/OPG ratio (Fig. 3A). Next, to confirm the indirect effects of IGU on osteoclast differentiation, we performed coculture experiments utilizing bone marrow-derived macrophages (BMDMs) and MLO-Y4 cells treated with IGU without adding RANKL. The coculture of BMDMs with MLO-Y4 cells promoted a notable increase in the number of multinuclear osteoclasts. Alternatively, IGU treatment in MLOY4 cells significantly decreased the number of multinuclear osteoclasts (Fig. 3B).

Evidence indicates that bone morphogenetic proteins (BMP) are signaling molecules that stimulate osteoblast differentiation and that sclerostin inhibits BMP-induced osteoblast differentiation [27~~26~~,30~~29~~]. RT-qPCR ~~resutls~~ results for the osteoblastic MC3T3-E1 cells showed that regardless of the presence of sclerostin, IGU significantly enhanced gene expression of ALP and osteocalcin (Fig. 3C). Furthermore, BMP6 administration promoted

ALP activity, whereas sclerostin inhibited ALP activity, with IGU administration restoring the inhibitory effects of sclerostin (Fig. 3D).

Studies have shown that Saos-2 cells are capable of differentiating into osteocyte-like cells and that BMP2 promotes the expression of sclerostin [26~~25~~,31~~30~~]. Our RT-qPCR ~~resutls~~ results revealed that BMP2 significantly increased the expression of osteocyte-related genes, including SOST and Dmp-1 (Fig. 3E), ~~alhtough~~ although IGU administration suppressed BMP2-induced expression of SOST and Dmp-1. However, BMP2 and IGU administration did not significantly change the expression of Dkk-1, another inhibitory factor of bone formation. Western blotting showed that IGU treatment dose-dependently suppressed sclerostin protein expression (Fig. 3F), whereas no alterations were observed in Dkk-1 expression (Supplementary Fig. 2).

Furthermore, to evaluate whether IGU influenced osteocyte apoptosis [32~~31~~,33~~32~~], we investigated the mitogen-activated protein kinase signaling pathway, including SAPK/JNK and p38, which regulates Saos-2 cell apoptosis. IGU treatment promoted the phosphorylation of SAPK/JNK and p38 (Fig. 3G). However, no difference in the empty lacunae ratio was observed among NS, HLU + NS, and HLU + IGU mice (Supplementary Fig. 3A). Moreover, in the intrinsic apoptotic pathway, IGU treatment slightly suppressed Caspase-9 but did not affect the expression of other genes in RT-qPCR (Supplementary Fig. 3B). In addition, the cell proliferation assay showed no significant differences regardless of the presence or absence of IGU (Supplementary Fig. 3C). Collectively, these findings suggest that IGU may not affect osteocyte apoptosis.

3.3 Effects of IGU on the NF-κB pathway in Saos-2 cells

To assess whether IGU treatment suppresses the transcriptional activation of the transcription factor NF-κB pathway, we investigated luciferase reporter assay using Saos-2

cells. Notably, TNFα administration significantly increased NF-κB transcriptional activity. Although IGU did not significantly affect NF-κB activity, dexamethasone significantly inhibited it (Fig. 4A).

Furthermore, we performed Western blotting with/without BMP2 and IGU to assess the effects of IGU administration on NF-κB translocation from the cytoplasm to the nucleus. Examination of the cytoplasm and nuclear protein contents of NF-κB through Western blotting revealed no remarkable difference (Fig. 4B). Moreover, immunofluorescence staining found that IGU administration did not significantly suppress NF-κB translocation from the cytoplasm to the nucleus (Fig. 4C). Collectively, these findings suggest that IGU may not affect the NF-κB pathway in osteocytes.

3.4 The potential of IGU to regulate EGR1 expression identified through RNA sequencing analysis in Saos-2 cells

To further investigate the possible mechanisms explaining the effects of IGU on osteocytes, we conducted RNA sequencing in Saos-2 cells from the untreated, BMP2-treated, and BMP2 + IGU-treated groups (Supplementary Fig. 4). ~~Notaobly~~Notably, screening of differentially expressed genes showed that IGU treatment effectively downregulated the expression levels of several genes known osteocyte-related genes, including SOST and Dmp1 (Fig. 5A). Next, Gene Ontology enrichment analysis revealed that IGU treatment primarily upregulated ossification regulation, skeletal system development, and collagen fibril organization but primarily downregulated cellular response to type Ⅰ interferon and the type Ⅰ interferon signaling pathway (Fig. 5B).

Figs. 5C and D ~~depicts~~ depict the top 10 genes differentially regulated in ascending order based on p values following IGU treatment. Among the top 10 genes, EGR1 is the only one classified as a regulation factor of DNA-templated transcription and has been reported to

be involved in mechanical stress [3433]. In anticipation of its relevance to the effects of IGU on osteocytes, we focused on this particualr particular gene. In fact, immunostaining of EGR1 in the distal femur revealed that the percentage of EGR1-positive osteocytes was higher in HLU + NS mice than in NS mice, with IGU treatment significantly attenuating this increase (Fig. 5E). Moreover, RT-qPCR revealed that in Saos-2 cells, BMP2 treatment with significantly increased EGR1 gene expression, whereaas whereas IGU treatment effectively suppressed the same EGR1 gene expression (Fig. 5F).

3.5 IGU treatment improves bone metabolism by regulating the ERK/EGR1/TNFα pathway

Studies have shown that mechanical unloading triggers the production of reactive oxygen species (ROS), which increase EGR1 transcriptional activity through the ERK pathway and downstream TNFα expression [3433,3534]. Moreover, other reports have suggested that heme oxygenase (HO)-1 was closely associated with ROS and that the expression of HO-1 increases by unloading [3635,3736]. In fact, immunostaining of HO-1 in the distal femur revealed that the number of HO-1-positive cells was higher in HLU + NS mice than in NS mice, with IGU treatment showing no significant effect (Fig. 6A). Therefore, we investigated the downstream ERK pathway, which is the downstream of ROS. Western blotting in Saos-2 cells showed that BMP2 promoted ERK1/2 phosphorylation, whereas IGU treatment inhibited this promotion (Fig. 6B). Next, we investigated downstream signals of ERK1/2 in osteocytes. Notably, immunostaining of TNFα in the distal femurs showed that the percentage of TNFα-positive osteocytes was significantly higher in the HLU + NS mice than in NS mice. Strikingly, IGU treatment significantly inhibited this increase (Fig. 6C). Thereafter, we further examined whether EGR1 overexpression induced TNFα and its downstream factors, such as RANKL and SOST expression, in osteocytes. Accordingly, we found that EGR1 overexpression

significantly increased not only TNFα expression but also RANKL and SOST expression (Fig. 6D). Furthermore, IGU treatment significantly inhibited all such increases. Moreover, RT-qPCR ~~analsis~~ analysis of EGR1-knockdown Saos-2 cells achieved through siEGR1 plasmid transfection revealed that siEGR1 transfection significantly reduced the expressions of RANKL and SOST by downregulating EGR1 expression (Fig. 6E).

A previous report suggested that an ion channel called Piezo1 was involved in the sensing of mechanical signals by osteocytes [38~~37~~]. Immunostaining of Piezo1 showed that HLU tended to downregulate the number of Piezo1-positive osteocytes, with IGU treatment showing no significant effects (Supplementary Fig. 5A). We further investigated the relationship between EGR1 and Piezo1. Accordingly, we found that EGR1 overexpression significantly increased the expression of Piezo1 and Cyr61, a target gene of YAP/TAZ downstream of Piezo1 (Supplementary Fig. 5B). In contrast, EGR1 knockdown showed no difference in the expression of Piezo1 and Cyr61 (Supplementary Fig. 5C).

Taken together, these findings suggest that IGU may inhibit the ERK/EGR1 pathway induced by mechanical unloading and consequent ROS production, thereby reducing osteocyte-expressed RANKL and SOST via TNFα suppression (Fig. 7). Besides the direct effect of IGU on osteoblasts and osteoclasts, these mechanisms may suppress osteoclastogenesis and enhance osteoblastogenesis under unloading conditions, which may ameliorate disuse osteoporosis.

4. Discussion

Previous reports have addressed the effects of IGU on postmenopausal osteoporosis model mice and its effects on bone metabolic disorders caused by glucocorticoids [20, 22]. However, to the best of our knowledge, no previous reports have focused on the effects of IGU on disuse osteoporosis. This study has been the first to demonstrate the detailed effects of IGU

in osteocytes and disuse osteoporosis.~~To the best of our knowledge, this study has been the first to demonstrate the detailed effects of IGU in osteocytes and disuse osteoporosis.~~ Our results revealed that IGU improved disuse osteoporosis in mice by inhibiting sclerostin and RANKL production through the ERK/EGR1/TNFα pathway in osteocytes.

Mechanical unloading on bone upregulates various cytokines, such as BMP2 and TNFα [28~~27~~,29~~28~~,39~~38~~]. Furthermore, TNFα induces RANKL expression in osteocytes, which play a major role in osteoclast differentiation [40~~39~~]. Sclerostin has been suggested to be another primary cause of disuse osteoporosis. In fact, studies have shown that SOST-deficient mice during hindlimb unloading were resistant to bone loss [32~~31~~] and that treating osteocytes with unloading-related factors, such as BMP2 and TNFα, significantly upregulated the transcriptional activity of the SOST [41~~40~~]. In our investigation, mechanical unloading promoted an increase in TNFα and sclerostin expression in osteocytes, which was suppressed by IGU treatment.

A previous study suggested that IGU improves bone metabolism ~~potentially~~ potentially through the inhibition of NF-κB [42~~41~~]. Moreoever, reports have shown that IGU may inhibit the activation of NF-κB by interfering with its translocation into the nucleus while not affecting the degradation of IκBα in THP-1 cells, a human monocytic leukemia cell line, and cultured human synovial cells [43~~42~~,44~~43~~]. However, these studies only evaluated the nuclear translocation of NF-κB and failed to show the transcriptional activity through luciferase assay like in the ~~currnet~~ current study. Given that the present study could not confirm the role of IGU in inhibiting NF-κB transcriptional activity in osteocytes, we conducted RNA sequencing to investigate the transcription factor EGR1, one of the key proteins involved in mechanical loading via the ROS/ERK pathway [34~~33~~]. Reports have ~~suggest~~ suggested that ~~that~~ unloading increases EGR1 expression in the tendon and muscles [34~~33~~,45~~44~~], although its expression in osteocytes remained unclear. In the current study, hindlimb-unloaded mice

showed an increase in EGR1 expression in osteocytes. Our results also showed that HO-1 in bone tissue ~~remaiend~~ remained unaltered despite IGU administration, suggesting that IGU did not affect ROS levels. Therefore, we focused on ERK, which is downstream of ROS, and found that IGU inhibited the ERK pathway, consistent with the findings of a previous report [46~~45~~]. EGR1 activates TNFα [36~~35~~,47~~46~~], with cases of disuse osteoporosis showing elevated expression levels of TNFα and downstream factors, such as RANKL and sclerostin, in cortical bone osteocytes [48~~47~~]. This suggests a strong association between unloading conditions and EGR1 within osteocytes. Finally, our results using EGR1 overexpression in osteocytes revealed that EGR1 upregulates TNFα and downstream RANKL and SOST expression, which was downregulated by IGU. Conversely, EGR1 downregulation by siEGR1 downregulated RANKL and SOST expression. These results strongly indicate that EGR1 plays crucial roles in the regulation of RANKL and SOST.

Recent studies have revealed that Piezo1, a mechanosensitive ion channel, is crucial for the skeletal response to mechanical loading in osteoblasts and osteocytes [38~~37~~,49~~48~~]. Piezo1 functions as a catalyst for Ca^{2+} influx in response to mechanical stimuli, subsequently governing downstream signaling cascades. Despite a previous report suggesting that extracellular Ca upregulated EGR1 [50~~49~~], the association between Piezo1 and EGR1 remains unclear. Our study suggested that EGR1 overexpression upregulated the expression of Piezo1 and its downstream genes, with EGR1 downregulation having no effect on these expressions. Taken together, our findings showed that enhanced EGR1 expression may induce Piezo1 compensation for the downregulation of mechanical loading-related signals by EGR1. However, siEGR1-induced downregulation of EGR1 or IGU treatment had no effect on Piezo1 and downstream gene expression, suggesting that IGU treatment and consequently EGR1 suppression were not associated with Piezo1.

This study has certain limitations worth noting. First, isolating and culturing

osteocytes from IGU-treated mice proved challenging. Furthermore, incorporating EGR1 knockout or transgenic mice was difficult in this experiment. Nevertheless, the study's strength lies in having been the first to elucidate the effects of IGUs on osteocytes using a mouse model of disuse osteoporosis.

5. Conclusion

Our findings suggest that IGU inhibited sclerostin and RANKL production through the ERK/EGR1/TNFα pathway in osteocytes, indicating its potential for becoming a unique and effective treatment option for disuse osteoporosis by targeting osteocytes.

Acknowledgment

We are grateful to M. Shinkawa, F. Hirayama, and Y. Eguchi for their excellent technical assistance. We thank all the members of Okada's laboratory for the helpful discussion and comments.

CRediT authorship

Declaration of conflicting interests

The iguratimod was kindly provided by Toyama Chemical Co., Ltd (Tokyo, Japan). K. Ebina has received research grants and lecture fees from Eisai Co., Ltd. K. Ebina, Y. Etani, and N. Ochiai are affiliated with, and K. Nakata supervises the Department of Musculoskeletal Regenerative Medicine, Osaka University Graduate School of Medicine, which is supported by Taisho Pharmaceutical Co., Ltd. N. Ochiai is an employee of Taisho Pharmaceutical Co., Ltd. These companies had no role in the study design, decision to publish, or preparation of the manuscript. T. Miura, M. Hirao, K. Takami, A. Goshima, T. Kurihara, Y. Fukuda, Y. Kanamoto, and S. Okada declare that they have no conflicts of interest.

Contribution statement

Taihei Miura: Conceptualization, Data curation, Methodology, Validation, Visualization, Formal analysis, Investigation, Resources, Writing - original draft. Yuki Etani: Conceptualization, Methodology, Supervision, Project administration. Takaaki Noguchi: Conceptualization, Methodology, Supervision, Project administration. Makoto Hirao: Conceptualization, Methodology, Supervision, Project administration. Kenji Takami: Investigation, Resources. Atsushi Goshima: Investigation, Resources. Takuya Kurihara: Investigation, Resources. Yuji Fukuda: Investigation, Resources. Nagahiro Ochiai: Investigation, Resources. Takashi Kanamoto: Supervision. Ken Nakata: Supervision. Seiji Okada: Supervision. Kosuke Ebina: Conceptualization, Methodology, Writing - review & editing, Visualization, Supervision, Project administration.

Availability of data and material

The data set used or analyzed in this study is available from the corresponding author upon reasonable request.

References

[1] J. Delgado-Calle, T. Bellido, The osteocyte as a signaling cell, Physiol Rev 102(1) (2022) 379-410. https://doi.org/10.1152/physrev.00043.2020

[2] L.F. Bonewald, The amazing osteocyte, J Bone Miner Res 26(2) (2011) 229-38. https://doi.org/10.1002/jbmr.320

[3] L. Wang, X. You, L. Zhang, C. Zhang, W. Zou, Mechanical regulation of bone remodeling, Bone Res 10(1) (2022) 16. https://doi.org/10.1038/s41413-022-00190-4

[4] M.P. Nagaraja, D. Risin, The current state of bone loss research: data from spaceflight and

551 microgravity simulators, J Cell Biochem 114(5) (2013) 1001-8.
552 https://doi.org/10.1002/jcb.24454
553 [5] E. Terpos, K. Fragiadaki, M. Konsta, C. Bratengeier, A. Papatheodorou, P.P. Sfikakis, Early
554 effects of IL-6 receptor inhibition on bone homeostasis: a pilot study in women with
555 rheumatoid arthritis, Clin Exp Rheumatol 29(6) (2011) 921-5.
556 [6] T. Rolvien, M. Amling, Disuse Osteoporosis: Clinical and Mechanistic Insights, Calcif
557 Tissue Int 110(5) (2022) 592-604. https://doi.org/10.1007/s00223-021-00836-1
558 [7] Y. Ma, W.S. Jee, Z. Yuan, W. Wei, H. Chen, S. Pun, H. Liang, C. Lin, Parathyroid hormone
559 and mechanical usage have a synergistic effect in rat tibial diaphyseal cortical bone, J Bone
560 Miner Res 14(3) (1999) 439-48. https://doi.org/10.1359/jbmr.1999.14.3.439
561 [8] K. Naruse, K. Uchida, M. Suto, K. Miyagawa, A. Kawata, K. Urabe, M. Takaso, M. Itoman,
562 Y. Mikuni-Takagaki, Alendronate does not prevent long bone fragility in an inactive rat model,
563 J Bone Miner Metab 34(6) (2016) 615-626. https://doi.org/10.1007/s00774-015-0714-y
564 [9] W. Balemans, M. Ebeling, N. Patel, E. Van Hul, P. Olson, M. Dioszegi, C. Lacza, W.
565 Wuyts, J.V. Den Ende, P. Willems, A.F. Paes-Alves, S. Hill, M. Bueno, F.J. Ramos, P.
566 Tacconi, F.G. Dikkers, C. Stratakis, K. Lindpaintner, B. Vickery, D. Foernzler, W. Van Hul,
567 Increased bone density in sclerosteosis is due to the deficiency of a novel secreted protein
568 (SOST), Hum Mol Genet 10(5) (2001) 537-43. https://doi.org/10.1093/hmg/10.5.537
569 [10] L. Qin, W. Liu, H. Cao, G. Xiao, Molecular mechanosensors in osteocytes, Bone Res 8
570 (2020) 23. https://doi.org/10.1038/s41413-020-0099-y
571 [11] A.E. Kearns, S. Khosla, P.J. Kostenuik, Receptor activator of nuclear factor kappaB ligand
572 and osteoprotegerin regulation of bone remodeling in health and disease, Endocr Rev 29(2)
573 (2008) 155-92. https://doi.org/10.1210/er.2007-0014
574 [12] J. Delgado-Calle, A.Y. Sato, T. Bellido, Role and mechanism of action of sclerostin in
575 bone, Bone 96 (2017) 29-37. https://doi.org/10.1016/j.bone.2016.10.007

[13] Y. Kobayashi, S. Uehara, N. Udagawa, N. Takahashi, Regulation of bone metabolism by Wnt signals, J Biochem 159(4) (2016) 387-92. https://doi.org/10.1093/jb/mvv124

[14] G.R. Heiland, K. Zwerina, W. Baum, T. Kireva, J.H. Distler, M. Grisanti, F. Asuncion, X. Li, M. Ominsky, W. Richards, G. Schett, J. Zwerina, Neutralisation of Dkk-1 protects from systemic bone loss during inflammation and reduces sclerostin expression, Ann Rheum Dis 69(12) (2010) 2152-9. https://doi.org/10.1136/ard.2010.132852

[15] K. Baek, H.R. Hwang, H.J. Park, A. Kwon, A.S. Qadir, S.H. Ko, K.M. Woo, H.M. Ryoo, G.S. Kim, J.H. Baek, TNF-alpha upregulates sclerostin expression in obese mice fed a high-fat diet, J Cell Physiol 229(5) (2014) 640-50. https://doi.org/10.1002/jcp.24487

[16] A.M. Dubrovsky, M.J. Lim, N.E. Lane, Osteoporosis in Rheumatic Diseases: Anti-rheumatic Drugs and the Skeleton, Calcif Tissue Int 102(5) (2018) 607-618. https://doi.org/10.1007/s00223-018-0401-9

[17] S. Siu, B. Haraoui, R. Bissonnette, L. Bessette, C. Roubille, V. Richer, T. Starnino, C. McCourt, A. McFarlane, P. Fleming, J. Kraft, C. Lynde, W. Gulliver, S. Keeling, J. Dutz, J.E. Pope, Meta-analysis of tumor necrosis factor inhibitors and glucocorticoids on bone density in rheumatoid arthritis and ankylosing spondylitis trials, Arthritis Care Res (Hoboken) 67(6) (2015) 754-64. https://doi.org/10.1002/acr.22519

[18] A. Hamar, Z. Szekanecz, A. Pusztai, M. Czokolyova, E. Vegh, Z. Petho, N. Bodnar, K. Gulyas, A. Horvath, B. Soos, L. Bodoki, H.P. Bhattoa, G. Nagy, G. Tajti, G. Panyi, E. Szekanecz, A. Domjan, K. Hodosi, S. Szanto, G. Szucs, S. Szamosi, Effects of one-year tofacitinib therapy on bone metabolism in rheumatoid arthritis, Osteoporos Int 32(8) (2021) 1621-1629. https://doi.org/10.1007/s00198-021-05871-0

[19~~18~~] L. Deng, F. Yao, F. Tian, X. Luo, S. Yu, Z. Wen, Influence of Iguratimod on Bone Metabolism in Patients with Rheumatoid Arthritis: A Meta-analysis, Int J Clin Pract 2022 (2022) 5684293. https://doi.org/10.1155/2022/5684293

[2019] Y.X. Wu, Y. Sun, Y.P. Ye, P. Zhang, J.C. Guo, J.M. Huang, X.Z. Jing, W. Xiang, S.Y. Yu, F.J. Guo, Iguratimod prevents ovariectomy‐induced bone loss and suppresses osteoclastogenesis via inhibition of peroxisome proliferator‐activated receptor‐γ, Mol Med Rep 16(6) (2017) 8200-8208. https://doi.org/10.3892/mmr.2017.7648

[2120] K. Kuriyama, C. Higuchi, K. Tanaka, H. Yoshikawa, K. Itoh, A novel anti-rheumatic drug, T-614, stimulates osteoblastic differentiation in vitro and bone morphogenetic protein-2-induced bone formation in vivo, Biochem Biophys Res Commun 299(5) (2002) 903-9. https://doi.org/10.1016/s0006-291x(02)02754-7

[2221] A. Miyama, K. Ebina, M. Hirao, G. Okamura, Y. Etani, K. Takami, A. Goshima, T. Miura, S. Oyama, T. Kanamoto, H. Yoshikawa, K. Nakata, Effects of iguratimod on glucocorticoid-induced disorder of bone metabolism in vitro, J Bone Miner Metab 39(4) (2021) 639-648. https://doi.org/10.1007/s00774-021-01206-5

[2322] T.J. Wronski, E.R. Morey-Holton, Skeletal response to simulated weightlessness: a comparison of suspension techniques, Aviat Space Environ Med 58(1) (1987) 63-8.

[2423] T. Noguchi, K. Ebina, M. Hirao, T. Morimoto, K. Koizumi, K. Kitaguchi, H. Matsuoka, T. Iwahashi, H. Yoshikawa, Oxygen ultra-fine bubbles water administration prevents bone loss of glucocorticoid-induced osteoporosis in mice by suppressing osteoclast differentiation, Osteoporos Int 28(3) (2017) 1063-1075. https://doi.org/10.1007/s00198-016-3830-1

[2524] Y. Etani, K. Ebina, M. Hirao, K. Kitaguchi, M. Kashii, T. Ishimoto, T. Nakano, G. Okamura, A. Miyama, K. Takami, A. Goshima, T. Kanamoto, K. Nakata, H. Yoshikawa, Combined effect of teriparatide and an anti-RANKL monoclonal antibody on bone defect regeneration in mice with glucocorticoid-induced osteoporosis, Bone 139 (2020) 115525. https://doi.org/10.1016/j.bone.2020.115525

[2625] L. Yu, M. van der Valk, J. Cao, C.Y. Han, T. Juan, M.B. Bass, C. Deshpande, M.A. Damore, R. Stanton, P. Babij, Sclerostin expression is induced by BMPs in human Saos-2

osteosarcoma cells but not via direct effects on the sclerostin gene promoter or ECR5 element, Bone 49(6) (2011) 1131-40. https://doi.org/10.1016/j.bone.2011.08.016

[2726] N. Kusu, J. Laurikkala, M. Imanishi, H. Usui, M. Konishi, A. Miyake, I. Thesleff, N. Itoh, Sclerostin is a novel secreted osteoclast-derived bone morphogenetic protein antagonist with unique ligand specificity, J Biol Chem 278(26) (2003) 24113-7. https://doi.org/10.1074/jbc.m301716200

[2827] G. Aleshcheva, M. Wehland, J. Sahana, J. Bauer, T.J. Corydon, R. Hemmersbach, T. Frett, M. Egli, M. Infanger, J. Grosse, D. Grimm, Moderate alterations of the cytoskeleton in human chondrocytes after short-term microgravity produced by parabolic flight maneuvers could be prevented by up-regulation of BMP-2 and SOX-9, FASEB J 29(6) (2015) 2303-14. https://doi.org/10.1096/fj.14-268151

[2928] X. Jin, H. Wang, X. Liang, K. Ru, X. Deng, S. Gao, W. Qiu, Y. Huai, J. Zhang, L. Lai, F. Li, Z. Miao, W. Zhang, A. Qian, Calycosin prevents bone loss induced by hindlimb unloading, NPJ Microgravity 8(1) (2022) 23. https://doi.org/10.1038/s41526-022-00210-x

[3029] M. Wu, G. Chen, Y.P. Li, TGF-beta and BMP signaling in osteoblast, skeletal development, and bone formation, homeostasis and disease, Bone Res 4 (2016) 16009. https://doi.org/10.1038/boneres.2016.9

[3130] M. Prideaux, A.R. Wijenayaka, D.D. Kumarasinghe, R.T. Ormsby, A. Evdokiou, D.M. Findlay, G.J. Atkins, SaOS2 Osteosarcoma cells as an in vitro model for studying the transition of human osteoblasts to osteocytes, Calcif Tissue Int 95(2) (2014) 183-93. https://doi.org/10.1007/s00223-014-9879-y

[3231] C. Lin, X. Jiang, Z. Dai, X. Guo, T. Weng, J. Wang, Y. Li, G. Feng, X. Gao, L. He, Sclerostin mediates bone response to mechanical unloading through antagonizing Wnt/beta-catenin signaling, J Bone Miner Res 24(10) (2009) 1651-61. https://doi.org/10.1359/jbmr.090411

[3332] K. Tanaka, T. Yamaguchi, I. Kanazawa, T. Sugimoto, Effects of high glucose and advanced glycation end products on the expressions of sclerostin and RANKL as well as apoptosis in osteocyte-like MLO-Y4-A2 cells, Biochem Biophys Res Commun 461(2) (2015) 193-9. https://doi.org/10.1016/j.bbrc.2015.02.091

[3433] T. Uchida, Y. Sakashita, K. Kitahata, Y. Yamashita, C. Tomida, Y. Kimori, A. Komatsu, K. Hirasaka, A. Ohno, R. Nakao, A. Higashitani, A. Higashibata, N. Ishioka, T. Shimazu, T. Kobayashi, Y. Okumura, I. Choi, M. Oarada, E.M. Mills, S. Teshima-Kondo, S. Takeda, E. Tanaka, K. Tanaka, M. Sokabe, T. Nikawa, Reactive oxygen species upregulate expression of muscle atrophy-associated ubiquitin ligase Cbl-b in rat L6 skeletal muscle cells, Am J Physiol Cell Physiol 314(6) (2018) C721-c731. https://doi.org/10.1152/ajpcell.00184.2017

[3534] J. Zhang, S. Xie, W. Ma, Y. Teng, Y. Tian, X. Huang, Y. Zhang, A newly identified microRNA, mmu-miR-7578, functions as a negative regulator on inflammatory cytokines tumor necrosis factor-alpha and interleukin-6 via targeting Egr1 in vivo, J Biol Chem 288(6) (2013) 4310-20. https://doi.org/10.1074/jbc.m112.351197

[3635] Y. Fang, C. Xing, X. Wang, H. Cao, C. Zhang, X. Guo, Y. Zhuang, R. Hu, G. Hu, F. Yang, Activation of the ROS/HO-1/NQO1 signaling pathway contributes to the copper-induced oxidative stress and autophagy in duck renal tubular epithelial cells, Sci Total Environ 757 (2021) 143753. https://doi.org/10.1016/j.scitotenv.2020.143753

[3736] R.B. Hunter, H. Mitchell-Felton, D.A. Essig, S.C. Kandarian, Expression of endoplasmic reticulum stress proteins during skeletal muscle disuse atrophy, Am J Physiol Cell Physiol 281(4) (2001) C1285-90. https://doi.org/10.1152/ajpcell.2001.281.4.c1285

[3837] X. Li, L. Han, I. Nookaew, E. Mannen, M.J. Silva, M. Almeida, J. Xiong, Stimulation of Piezo1 by mechanical signals promotes bone anabolism, Elife 8 (2019). https://doi.org/10.7554/elife.49631

[3938] Y. Yan, L. Wang, L. Ge, J.L. Pathak, Osteocyte-Mediated Translation of Mechanical

Stimuli to Cellular Signaling and Its Role in Bone and Non-bone-Related Clinical Complications, Curr Osteoporos Rep 18(1) (2020) 67-80. https://doi.org/10.1007/s11914-020-00564-9

[40~~39~~] J. Xiong, M. Onal, R.L. Jilka, R.S. Weinstein, S.C. Manolagas, C.A. O'Brien, Matrix-embedded cells control osteoclast formation, Nat Med 17(10) (2011) 1235-41. https://doi.org/10.1038/nm.2448

[41~~40~~] A. Sebastian, G.G. Loots, Transcriptional control of Sost in bone, Bone 96 (2017) 76-84. https://doi.org/10.1016/j.bone.2016.10.009

[42~~41~~] C.H. Li, Z.Z. Ma, L.L. Jian, X.Y. Wang, L. Sun, X.Y. Liu, Z.Q. Yao, J.X. Zhao, Iguratimod inhibits osteoclastogenesis by modulating the RANKL and TNF-alpha signaling pathways, Int Immunopharmacol 90 (2021) 107219. https://doi.org/10.1016/j.intimp.2020.107219

[43~~42~~] Y. Aikawa, M. Yamamoto, T. Yamamoto, K. Morimoto, K. Tanaka, An anti-rheumatic agent T-614 inhibits NF-κB activation in LPS- and TNF-α-stimulated THP-1 cells without interfering with IκBα degradation, Inflamm Res 51(4) (2002) 188-94. https://doi.org/10.1007/pl00000291

[44~~43~~] M. Kohno, Y. Aikawa, Y. Tsubouchi, A. Hashiramoto, R. Yamada, Y. Kawahito, K. Inoue, Y. Kusaka, M. Kondo, H. Sano, Inhibitory effect of T-614 on tumor necrosis factor-alpha induced cytokine production and nuclear factor-kappaB activation in cultured human synovial cells, J Rheumatol 28(12) (2001) 2591-6.

[45~~44~~] A. Herchenhan, F. Dietrich-Zagonel, P. Schjerling, M. Kjaer, P. Eliasson, Early Growth Response Genes Increases Rapidly After Mechanical Overloading and Unloading in Tendon Constructs, J Orthop Res 38(1) (2020) 173-181. https://doi.org/10.1002/jor.24513

[46~~45~~] Y. Wei, X. Sun, M. Hua, W. Tan, F. Wang, M. Zhang, Inhibitory Effect of a Novel Antirheumatic Drug T-614 on the IL-6-Induced RANKL/OPG, IL-17, and MMP-3 Expression

in Synovial Fibroblasts from Rheumatoid Arthritis Patients, Biomed Res Int 2015 (2015) 214683. https://doi.org/10.1155/2015/214683

[4746] L. Shi, R. Kishore, M.R. McMullen, L.E. Nagy, Lipopolysaccharide stimulation of ERK1/2 increases TNF-alpha production via Egr-1, Am J Physiol Cell Physiol 282(6) (2002) C1205-11. https://doi.org/10.1152/ajpcell.00511.2001

[4847] C.E. Metzger, S. Anand Narayanan, P.H. Phan, S.A. Bloomfield, Hindlimb unloading causes regional loading-dependent changes in osteocyte inflammatory cytokines that are modulated by exogenous irisin treatment, NPJ Microgravity 6 (2020) 28. https://doi.org/10.1038/s41526-020-00118-4

[4948] W. Sun, S. Chi, Y. Li, S. Ling, Y. Tan, Y. Xu, F. Jiang, J. Li, C. Liu, G. Zhong, D. Cao, X. Jin, D. Zhao, X. Gao, Z. Liu, B. Xiao, Y. Li, The mechanosensitive Piezo1 channel is required for bone formation, Elife 8 (2019). https://doi.org/10.7554/elife.47454

[5049] G. Thiel, A. Lesch, A. Keim, Transcriptional response to calcium-sensing receptor stimulation, Endocrinology 153(10) (2012) 4716-28. https://doi.org/10.1210/en.2012-1343

Figure legends

Figure 1. Effects of iguratimod on disuse osteoporosis in hindlimb-unloaded (HLU) mice. (A) Experimental protocol. (B) Body weight changes (in grams) in mice of each group. (C) Representative microcomputed tomography images of the distal femur in the three groups after the intervention. Scale bar: 500 μm. (D) Quantification of trabecular bone parameters: bone volume (BV)/tissue volume (TV), trabecular number (Tb.N), trabecular thickness (Tb.Th), and trabecular separation (Tb.Sp). One-way ANOVA followed by Tukey's post-hoc analysis, **p < 0.01, *p < 0.05 (vs. HLU mice). All data were expressed as mean ± standard deviation for eight mice in each group.

Figure 2. Histological and histomorphometrical analyses of the distal femur for osteoclasts, osteoblasts, and osteocytes in normal saline (NS) and hindlimb-unloaded (HLU) mice with or without iguratimod (IGU) 5 days per week for 3 weeks.

(A–C) Representative histological findings of trabecular and cortical bone in the distal femur were examined using Tartrate-resistant acid phosphatase (TRAP) staining (A) and immunohistochemical stains of osteocalcin (red arrows indicate osteocalcin-positive cells) (B) and sclerostin (black arrows indicate sclerostin-positive osteocytes) (C) in each group (NS, HLU + NS, and HLU + IGU). Scale bars: A 100 μm, B,C 50 μm. (D and E) Villanueva bone staining of trabecular and cortical bone in the distal femur was conducted. The secondary cancellous bone area was stained in green through computer image processing, whereas the trabecular bone was stained in orange through computer image processing (D). Villanueva bone staining was conducted under fluorescent light (E). Osteoclasts and trabecular bone were stained in pink through computer image processing (G). Scale bars: D 500 μm; E 100 μm; F 10 μm. Trabecular bone parameters, including bone formation rate per total volume (BFR/TV) and erosion surface/bone surface (ES/BS) were quantified (F and H). One-way ANOVA followed by Tukey's post-hoc analysis, $^{**}p < 0.01$, $^{*}p < 0.05$ (vs. HLU mice). All data were expressed as the mean ± standard deviation (A–C; n = 8, F and H; n = 3)

Figure 3. Effects of iguratimod (IGU) on osteocytes and osteoclastogenesis/osteoblastogenesis through osteocytes in vitro.

(A) Effects of IGU on osteoclast-related gene expression in MLO-Y4 cells after tumor necrosis factor (TNF)-α stimulation were analyzed using RT-qPCR analysis (data from three independent experiments for each group). (B) Investigation of the effects of IGU on osteoclast formation in cocultures of TNFα-stimulated MLO-Y4 and bone marrow cells as osteoclast precursors (data from five to six independent experiments for each group). Scale bar: 500 μm.

(C) RT-qPCR analysis of osteoblast-related gene expression in MC3T3-E1 cells treated with BMP6 and sclerostin with or without IGU (data from three independent experiments for each group). (D) Alkaline phosphatase (ALP) activity was measured using MC3T3-E1 cells cultured with BMP6 and sclerostin with or without IGU (data from three independent experiments for each group). (E) Effects of IGU on osteocyte-related gene expression in Saos-2 cells after BMP2 stimulation were analyzed using RT-qPCR analysis (data from three independent experiment data for each group). (F) Western blotting analysis of SOST using Saos-2 cells treated with BMP2 with or without IGU. (G) Effects of IGU on the mitogen-activated protein kinases signaling pathway in Saos-2 cells after BMP2 stimulation were analyzed using Western blotting analysis. Statistical significance was determined using one-way ANOVA followed by Tukey's post-hoc test (**$p < 0.01$, *$p < 0.05$). All data are presented as the mean ± standard deviation.

Figure 4. Effects of iguratimod (IGU) on the NF-κB pathway in Saos-2 cells.

(**A**) Luciferase assay performed on Saos-2 cells cultured with TNFα/BMP2 with or without IGU/dexamethasone (Dex). NF-κB luciferase activity was expressed relative to that of the control, set at 100% (data from five to seven independent experiments for each group). (**B**) Western blotting analysis of p-p65 and p65 using nuclear and cytosolic proteins extracted from Saos-2 cells cultured with BMP2 with or without IGU. β-actin and Lamin B1 were used as the internal controls for the cytosolic and nuclear fractions, respectively. (**C**) Effects of IGU on the nuclear translocation of NF-κB p65 using immunofluorescence staining in Saos-2 cells cultured with BMP2 with or without IGU. Scale bars: 30 μm. The quantification of nuclear-cytoplasmic intensity ratios was normalized to the control, set at 100 (data from eight independent experiments for each group). Statistical significance was determined using one-way ANOVA followed by Tukey's post-hoc test (**$p < 0.01$, *$p < 0.05$). All data are presented

as the mean ± standard deviation.

Figure 5. Potential of iguratimod to regulate early growth response protein 1 (EGR1) expression identified through RNA sequencing analysis on Saos-2 cells.

(**A**) This heat map visualizes the expression levels of differentially expressed genes identified from RNA-seq datasets between BMP2-treated and BMP2 + IGU-treated groups. Green represents replicates with low expression, whereas red represents those with high expression. (**B**) Gene Ontology analysis of functional annotations for biological processes upregulated and downregulated by IGU treatment. (**C**) The top 10 transcription factor genes whose expression was significantly altered by IGU treatment. (**D**) Volcano plot displaying the differentially expressed transcripts between the BMP2-treated and BMP2 + IGU-treated groups. (**E)** Immunohistochemical staining of EGR1 in the distal femur cortical bone of each group (NS, HLU + NS, and HLU + IGU) (data from eight independent experiments for each group). The black arrows indicate EGR1-positive osteocytes. (**F**) RT-qPCR analysis of EGR1 gene expression was performed using Saos-2 cells treated with or without BMP2 and IGU (data from three independent experiments for each group). Statistical significance was determined using one-way ANOVA followed by Tukey's post-hoc test (**$p < 0.01$, *$p < 0.05$). All data are presented as the mean ± standard deviation.

Figure 6. Effects of iguratimod (IGU) on the production of sclerostin and RANKL from osteocytes through the ERK/EGR1/TNFα pathway.

(**A)** Immunohistochemical staining of heme oxygenase (HO)-1 in the distal femur of each group (NS, HLU + NS, and HLU + IGU) (data from seven to eight independent experiments for each group). (**B**) Western blotting analysis of ERK1/2 was performed on Saos-2 cells treated with or without BMP2 and IGU. (**C)** Immunohistochemical staining of TNFα in the distal

femur cortical bone of each group (NS, HLU + NS, and HLU + IGU) (data from seven to eight independent experiments for each group). The red arrows indicate TNFα-positive osteocytes. (**D**) Saos-2 cells were transiently transfected with the EGR1 overexpression vector and treated with or without IGU. RT-qPCR analysis of EGR1, TNFα, and osteocyte-related gene expression (data from three independent experiment data for each group). (**E**) Saos-2 cells were transiently transfected with EGR1-specific siRNA. RT-qPCR analysis of EGR1 and osteocyte-related gene expression (data from three independent experiment data for each group). An unpaired Student's t-test was employed for comparisons between two groups, whereas one-way ANOVA followed by Tukey's post-hoc test was used for comparisons between more than three groups. All data are expressed by the mean ± standard deviation. Differences were considered relevant at $p < 0.05$ (*$p < 0.05$, **$p < 0.01$).

Figure 7. Hypothetic scheme summarizing the effects of iguratimod (IGU).
Mechanical unloading may induce reactive oxygen species (ROS) and activate the downstream ERK/EGR1/TNFα pathway in osteocytes. IGU may inhibit the phosphorylation of ERK1/2 and downstream EGR1/TNFα pathway, thereby suppressing the expression of RANKL and sclerostin, potentially ameliorating disuse osteoporosis.

~~**Supplemental Figure 1. Effects of iguratimod on cortical bone loss in hindlimb-unloaded (HLU) mice.**~~

~~(**A**) Tail-suspended hindlimb-unloaded mice confined in the cage, demonstrating the suspension system. (**B**) Representative microcomputed tomography images of the distal femur in the three groups after the intervention. Scale bars: 500 μm. (**C**) Quantification of the cortical bone parameter: cortical thickness (Ct.Th). One-way ANOVA followed by Tukey's post-hoc analysis, **p < 0.01 (vs. HLU mice). All data were expressed as mean ± standard deviation for~~

eight mice in each group.

Supplemental Figure 2. Effects of iguratimod (IGU) on osteocyte-related gene, Dkk-1 expression.

Western blotting analysis of Dkk-1 using Saos-2 cells treated with bone morphogenetic protein-2 with or without IGU.

Supplemental Figure 3. Effects of iguratimod (IGU) on osteocyte apoptosis.

(**A**) Quantification of the relative number of empty lacunae in the cortical bone of the distal femur obtained from each group (normal saline (NS), hindlimb-unloaded (HLU) + NS, and HLU + IGU). The black arrows indicate the empty lacunae. (**B**) Reverse transcription quantitative polymerase chain reaction analysis of apoptosis-related gene expression in Saos-2 cells treated with bone morphogenetic protein-2 (BMP2) with or without IGU (data from three independent experiment data for each group). (**C**) Evaluation of cell proliferation in Saos-2 cells treated with different concentrations of IGU in the presence of BMP2 (data from five to six independent experiments for each group). Statistical significance was determined using one-way ANOVA followed by Tukey's post-hoc test (*$p < 0.05$). All data are presented as mean ± standard deviation.

Supplemental Figure 4. The heatmap of differentially expressed genes, which were detected by RNA sequencing analysis on Saos-2 cells from untreated, bone morphogenetic protein-2 (BMP2)-treated, and BMP2 + iguratimod (IGU)-treated groups.

Hierarchical clustering analysis was performed to generate a gene expression profile map of Saos-2 cells under untreated conditions, as well as conditions treated with BMP2 or BMP2 + IGU. The gene expression levels are represented by different colors: red points indicate up-

regulated genes, green points indicate down-regulated genes and black points represent genes with no change in expression.

Supplemental Figure 5. Effects of iguratimod (IGU) on Piezo1-related genes. (**A**) Immunohistochemical staining of Piezo1 in the distal femur cortical bone of each group (normal saline (NS), hindlimb-unloaded (HLU) + NS, and HLU + IGU) (data eight independent experiments for each group). The black arrows indicate Piezo1-positive osteocytes. (**B and C**) Saos-2 cells were transiently transfected with the early growth response protein 1 (EGR1) overexpression vector (**B**) and the EGR1-specific siRNA (**C**). Reverse transcription quantitative polymerase chain reaction analysis was conducted to examine the expression of EGR1 and Piezo1-related genes (data from three independent experiment data for each group). Statistical significance was assessed using one-way ANOVA followed by Tukey's post-hoc test (**p < 0.01). All data are expressed as the mean ± standard deviation.

Figure 1

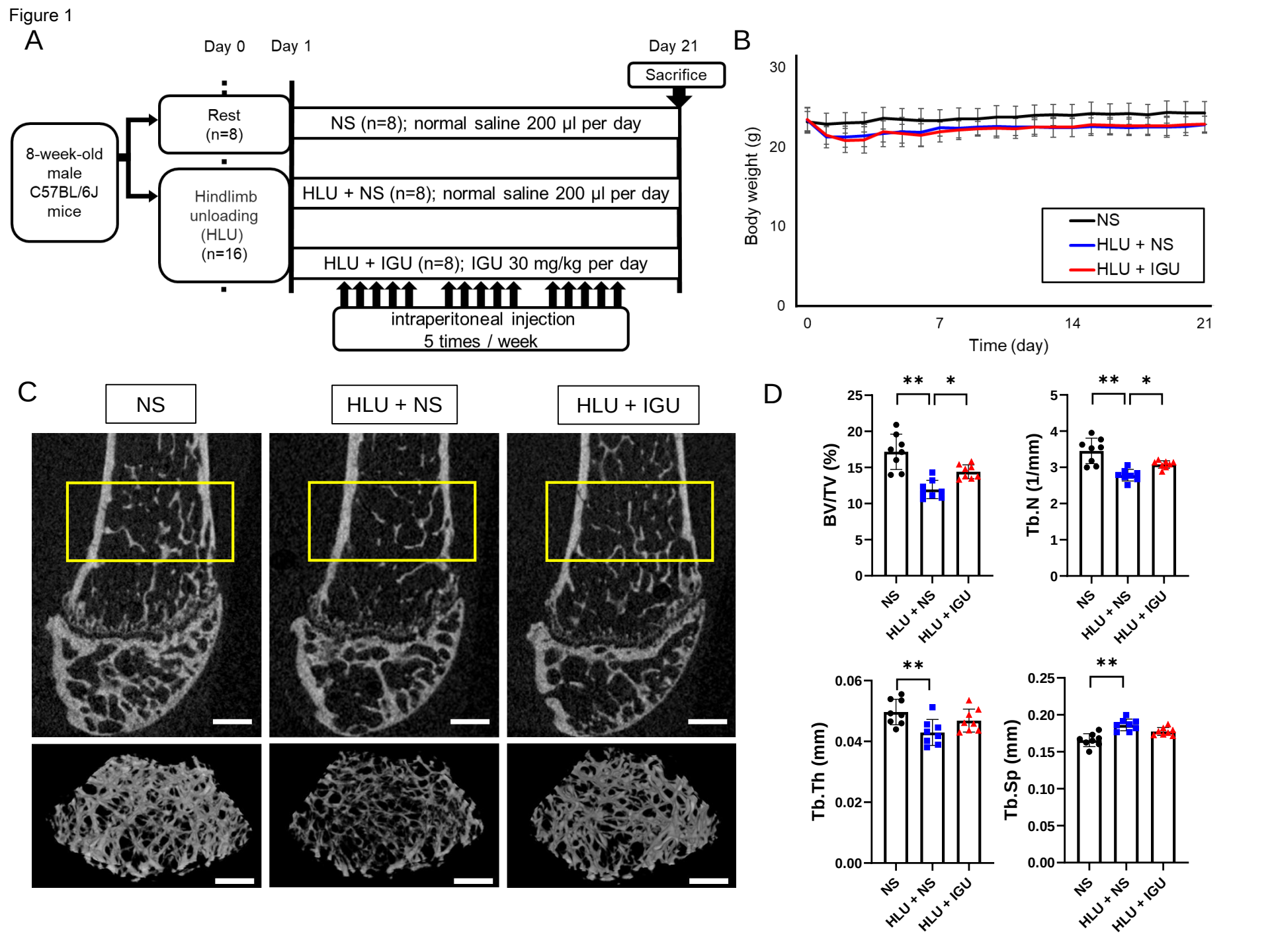
A
Day 0
Day 1
Day 21
Sacrifice
8-week-old male C57BL/6J mice
Rest (n=8)
Hindlimb unloading (HLU) (n=16)
NS (n=8); normal saline 200 µl per day
HLU + NS (n=8); normal saline 200 µl per day
HLU + IGU (n=8); IGU 30 mg/kg per day
intraperitoneal injection 5 times / week
B
Body weight (g)
Time (day)
NS
HLU + NS
HLU + IGU
C
NS
HLU + NS
HLU + IGU
D
BV/TV (%)
Tb.N (1/mm)
Tb.Th (mm)
Tb.Sp (mm)

Figure 2

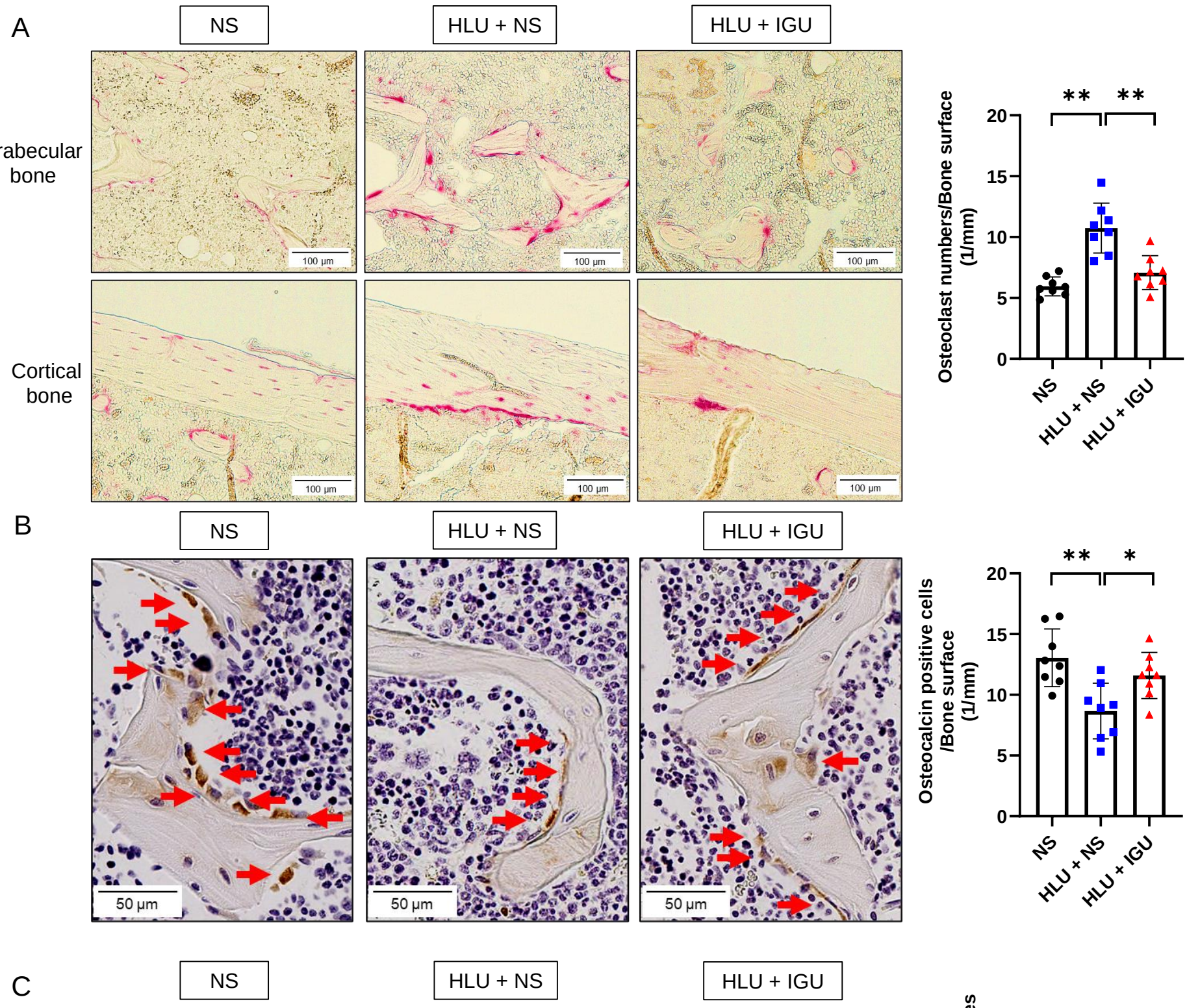
A
NS
HLU + NS
HLU + IGU
Trabecular bone
Cortical bone
100 μm
B
50 μm
C
D
500 μm
E
100 μm
G
10 μm
Osteocalcin positive cells /Bone surface (1/mm)
% sclerostin positive osteocytes
BFR/TV (%/year)
ES/BS (%)
ns
F
H

Figure 3

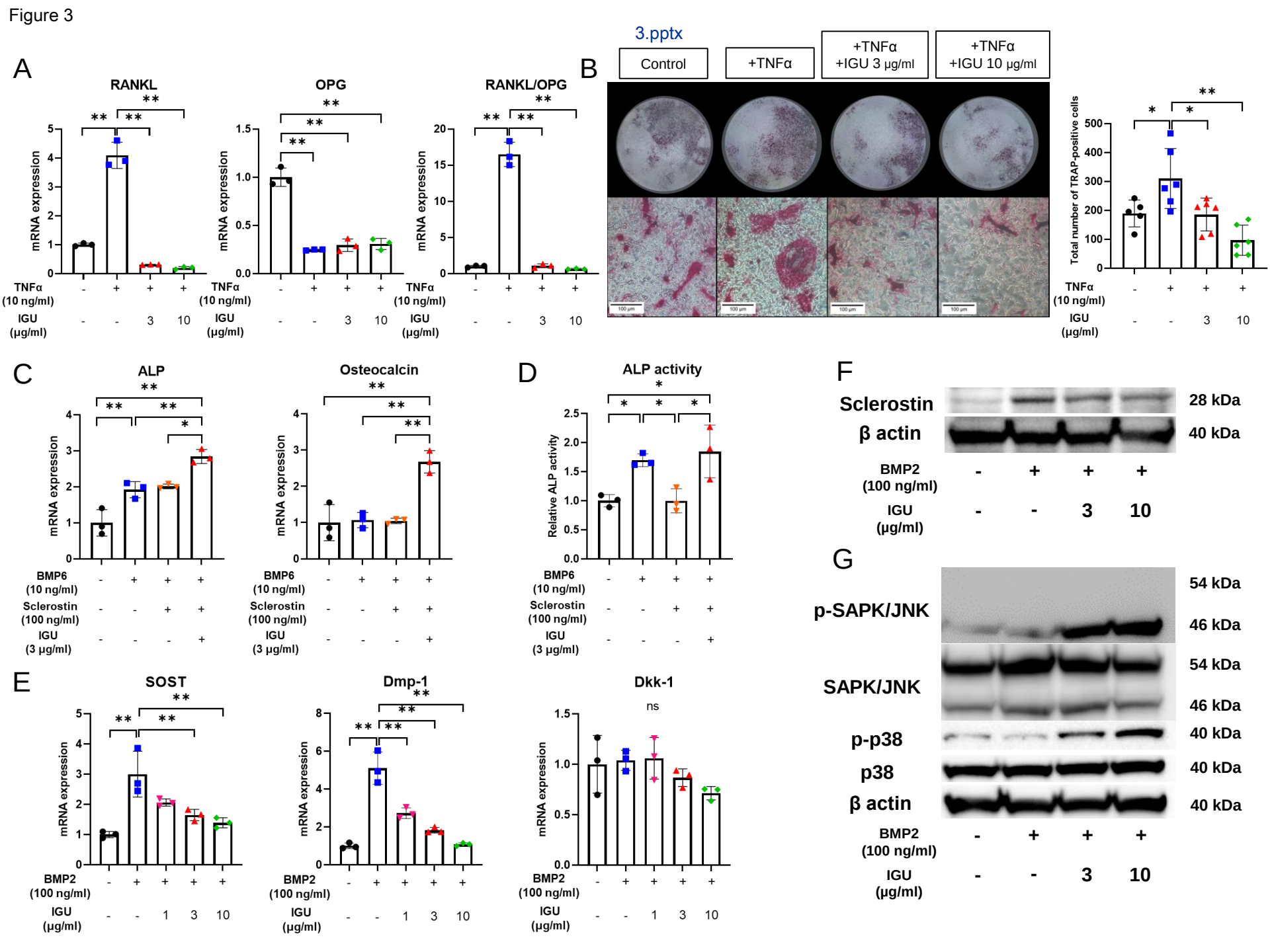
A
RANKL
OPG
RANKL/OPG
mRNA expression
TNFα (10 ng/ml)
IGU (μg/ml)
B
3.pptx
Control
+TNFα
+TNFα +IGU 3 μg/ml
+TNFα +IGU 10 μg/ml
Total number of TRAP-positive cells
C
ALP
Osteocalcin
BMP6 (10 ng/ml)
Sclerostin (100 ng/ml)
IGU (3 μg/ml)
D
ALP activity
Relative ALP activity
E
SOST
Dmp-1
Dkk-1
ns
BMP2 (100 ng/ml)
IGU (μg/ml)
F
Sclerostin
β actin
28 kDa
40 kDa
BMP2 (100 ng/ml)
IGU (μg/ml)
G
p-SAPK/JNK
SAPK/JNK
p-p38
p38
β actin
54 kDa
46 kDa
40 kDa

Figure 4

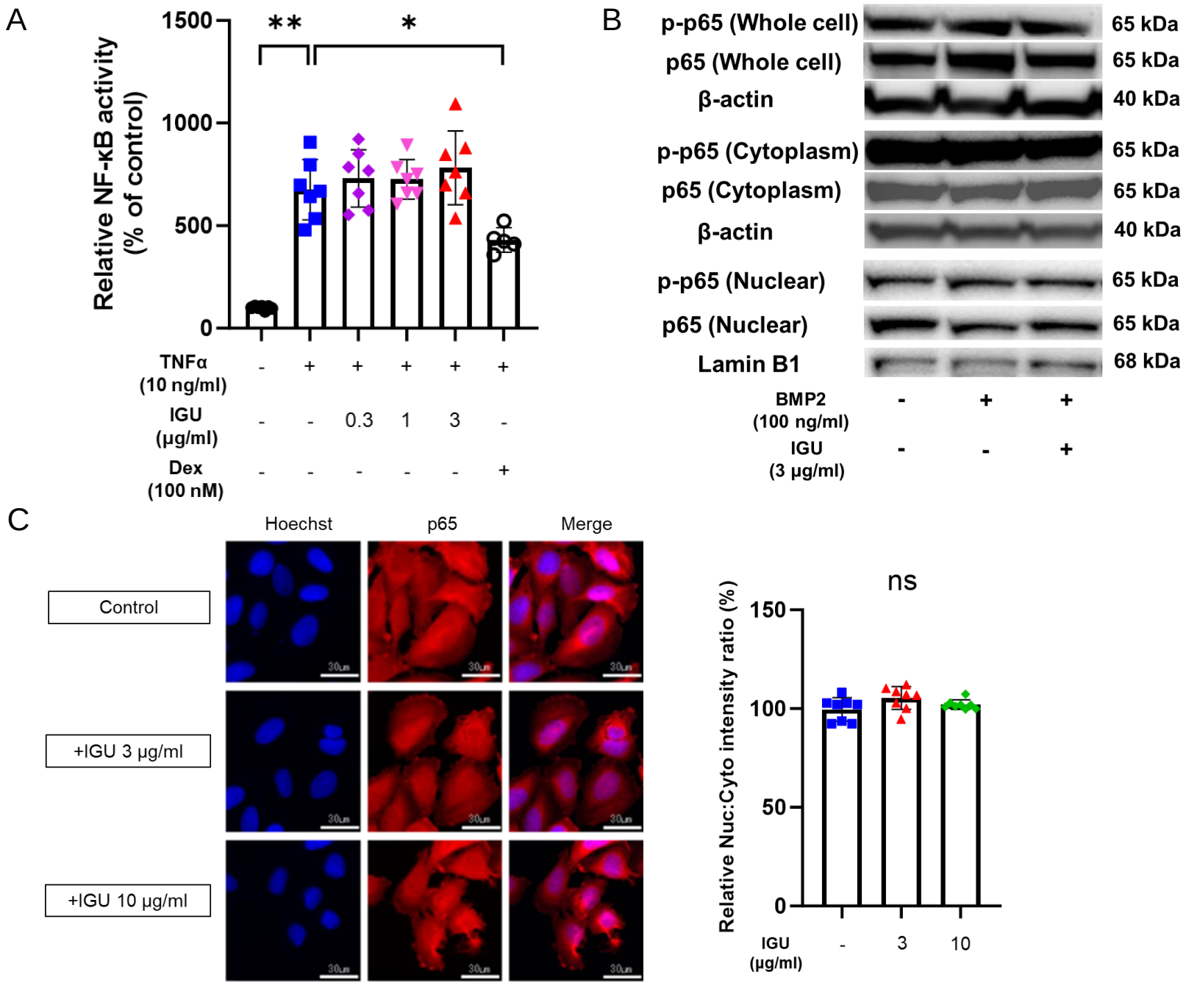
A
Relative NF-κB activity (% of control)
1500
1000
500
0
**
*
TNFα (10 ng/ml)
IGU (μg/ml)
Dex (100 nM)
B
p-p65 (Whole cell)
p65 (Whole cell)
β-actin
p-p65 (Cytoplasm)
p65 (Cytoplasm)
β-actin
p-p65 (Nuclear)
p65 (Nuclear)
Lamin B1
65 kDa
40 kDa
68 kDa
BMP2 (100 ng/ml)
IGU (3 μg/ml)
C
Hoechst
p65
Merge
Control
+IGU 3 μg/ml
+IGU 10 μg/ml
ns
Relative Nuc:Cyto intensity ratio (%)
150
100
50
0
IGU (μg/ml)

Figure 5

A

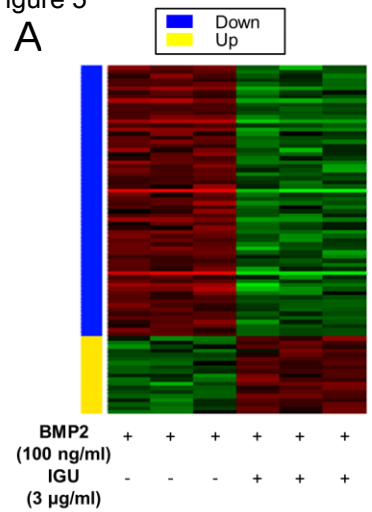

B

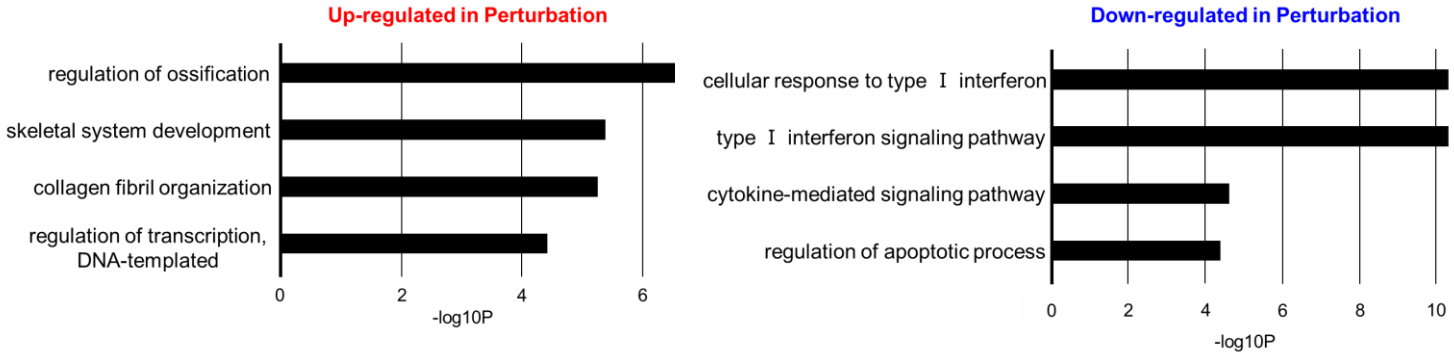

C

Gene	logFC	AveExpr	P-value	FDR	GO Biological Process
MEPE	-2.06	4.26	6.98E-15	9.67E-11	skeletal system development
DMP1	-2.09	4.52	1.61E-14	1.11E-10	ossification
EGR1	-1.59	5.60	4.75E-14	2.20E-10	regulation of dna-templated transcription
PLEKHA6	-1.25	6.63	1.11E-13	3.84E-10	N/A
TAC3	-1.23	6.40	5.03E-13	1.27E-09	signaling (neuropeptide)
SOST	-0.80	10.19	5.51E-13	1.27E-09	signaling (Wnt, BMP)
IBSP	-1.04	7.38	7.60E-13	1.50E-09	cell adhesion
KCNN3	-0.75	8.39	1.28E-11	2.22E-08	ion transport
IGFBP5	0.92	6.21	3.94E-11	6.07E-08	signaling (insulin-like growth factor)
FRZB	-1.44	3.99	5.59E-11	7.75E-08	signaling (Wnt)

D

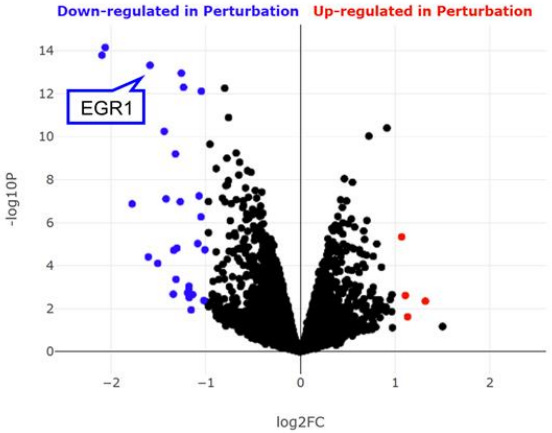

E

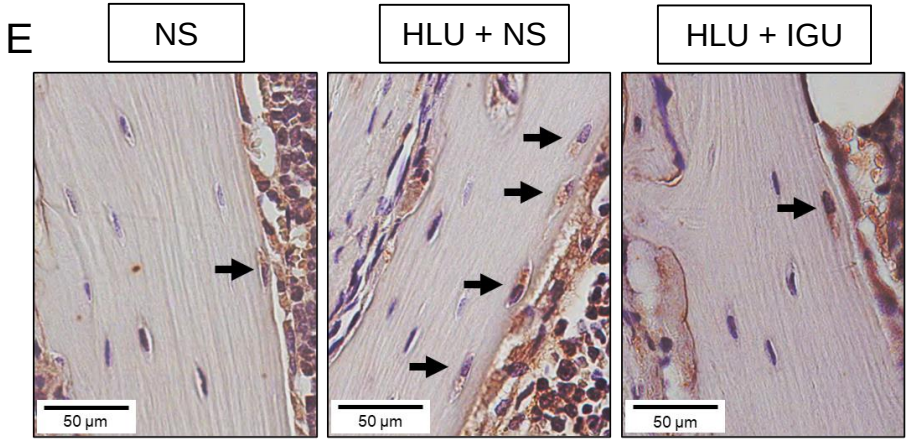

F

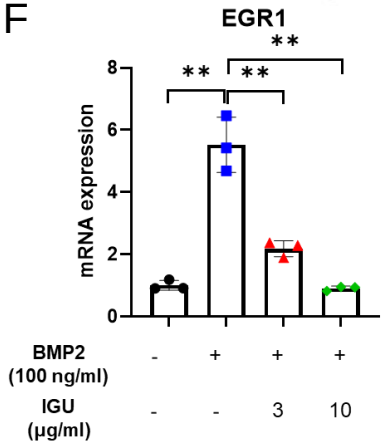

Figure 6

A

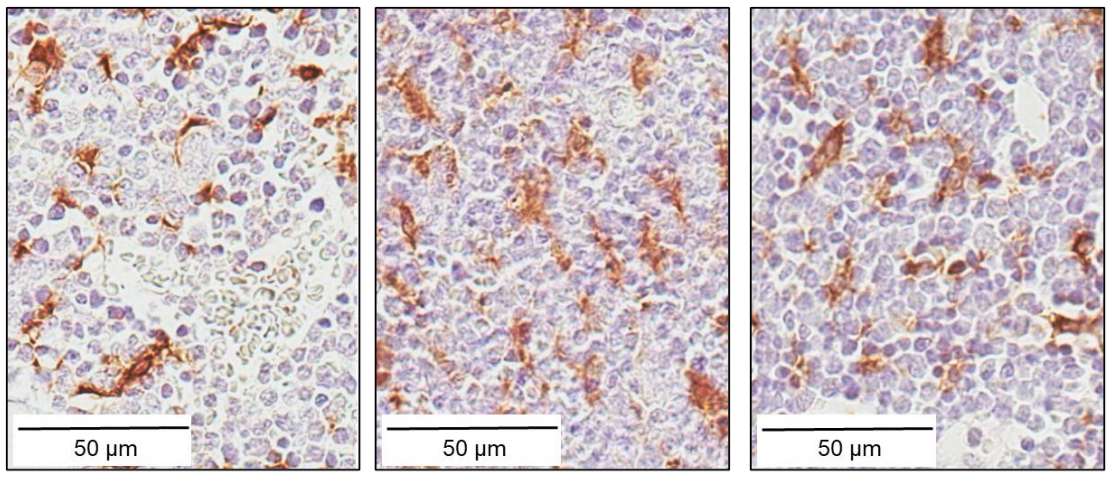

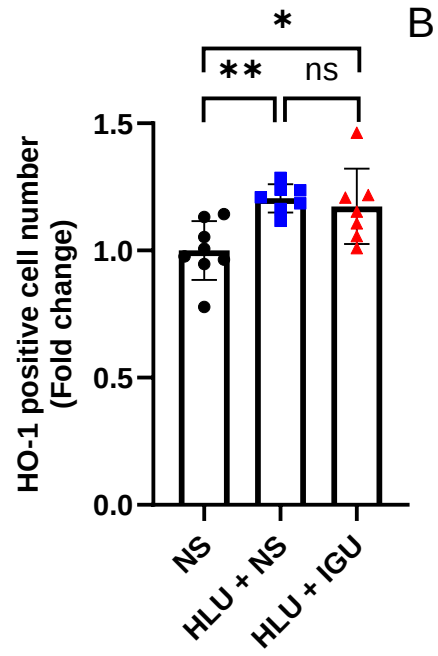

B

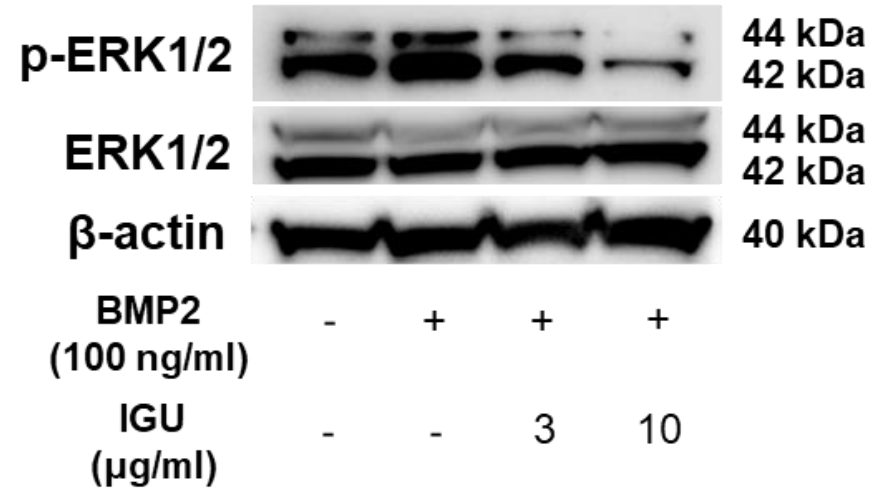

C

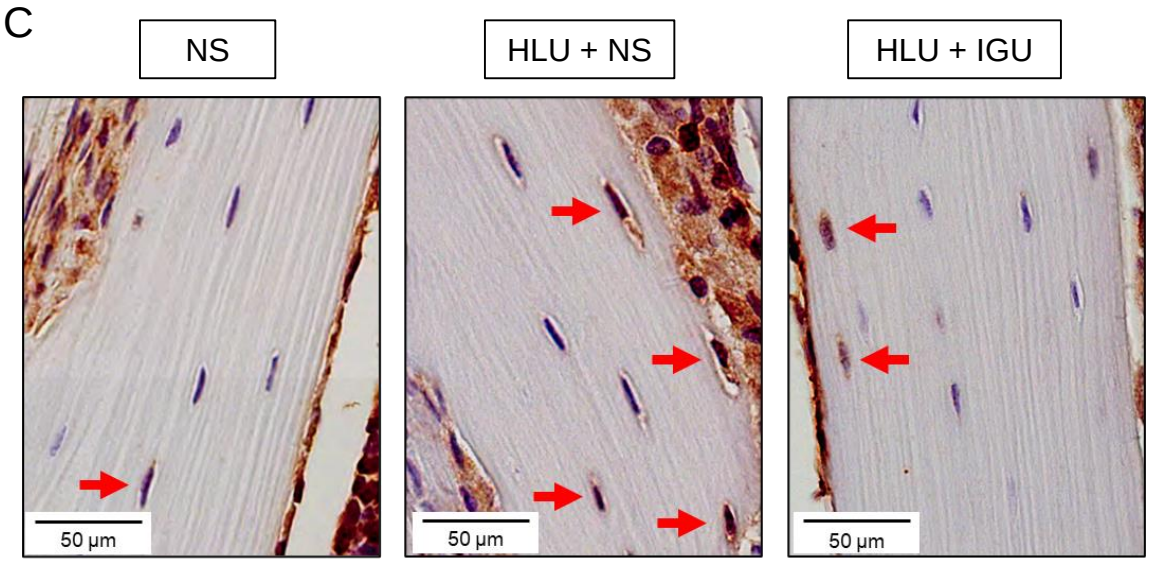

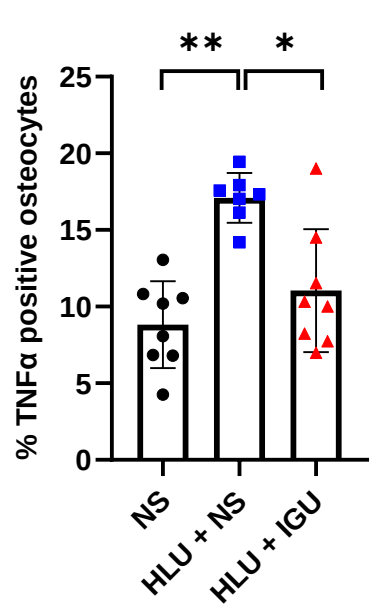

D

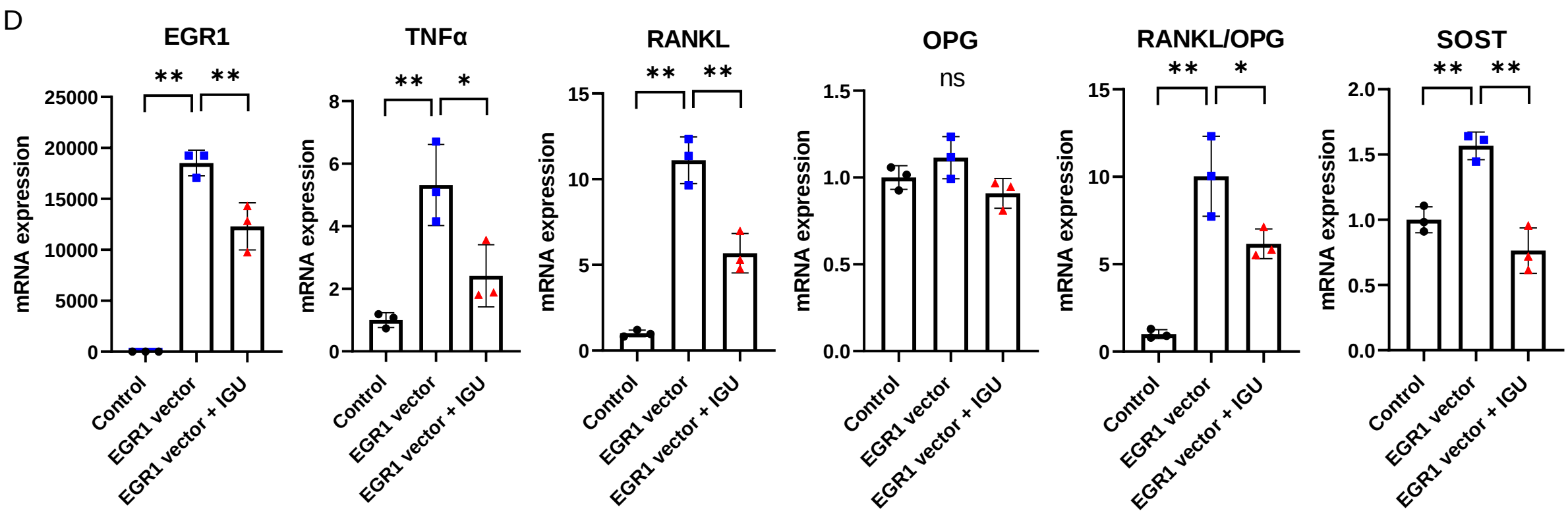

E

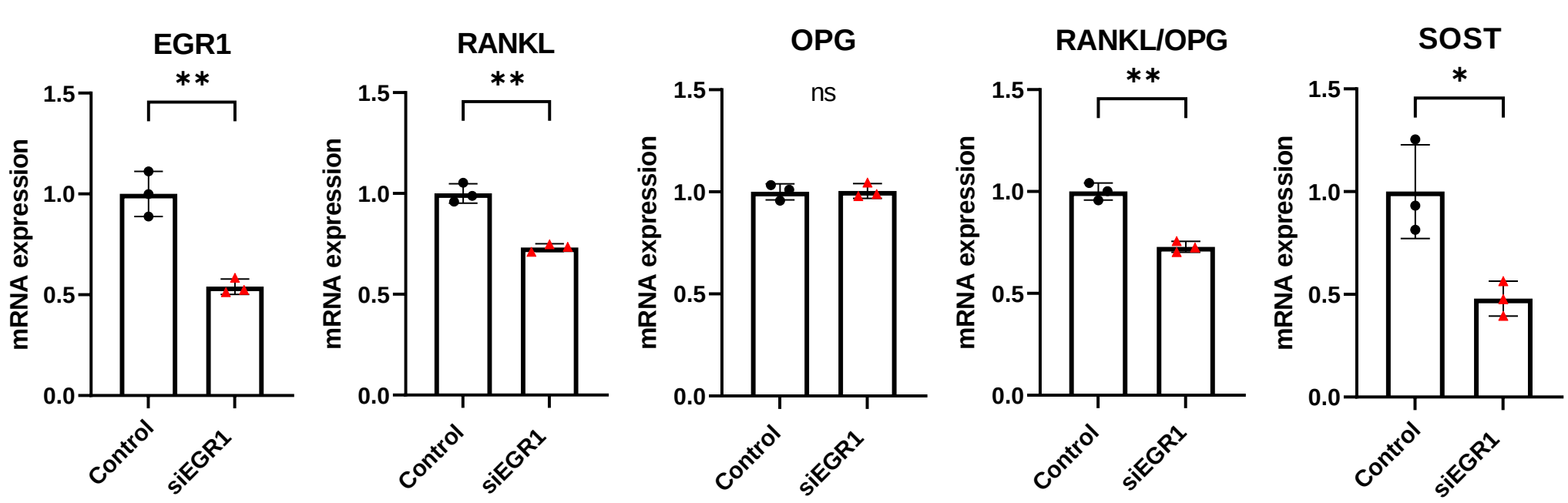

Figure 7

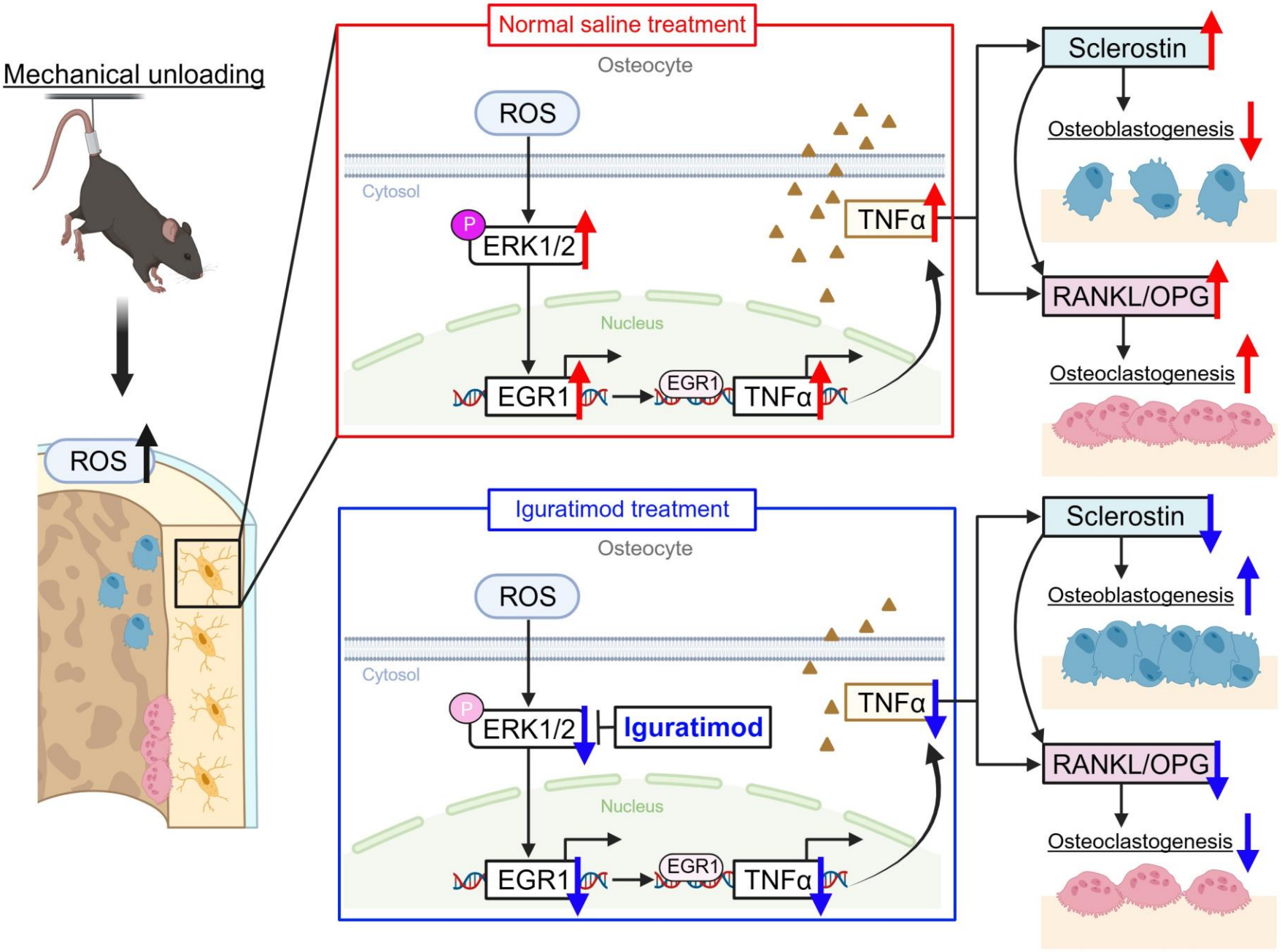
Mechanical unloading
ROS
Normal saline treatment
Osteocyte
ROS
Cytosol
P
ERK1/2
TNFα
Nucleus
EGR1
EGR1
TNFα
Sclerostin
Osteoblastogenesis
RANKL/OPG
Osteoclastogenesis
Iguratimod treatment
Osteocyte
ROS
Cytosol
P
ERK1/2
Iguratimod
TNFα
Nucleus
EGR1
EGR1
TNFα
Sclerostin
Osteoblastogenesis
RANKL/OPG
Osteoclastogenesis